Pergamon

Geochimica et Cosmochimica Acta, Vol. 66, No. 21, pp. 3733–3756, 2002

0016-7037/02 $22.00 + .00

PII S0016-7037(01)00884-5

Chemical evolution of seawater during the Phanerozoic: Implications from the record of marine evaporites

JUSKE HORITA,[1,*] HEIDE ZIMMERMANN,[2] and HEINRICH D. HOLLAND[2]

[1]Chemical Sciences Division, Oak Ridge National Laboratory, Oak Ridge, TN 37831-6110, USA
[2]Department of Earth and Planetary Sciences, Harvard University, 20 Oxford Street, Cambridge, MA 02138, USA

(*Received March* 22, 2001; *accepted in revised form November* 27, 2001)

Abstract—The chemical evolution of seawater during the Phanerozoic is still a matter of debate. We have assembled and critically analyzed the available data for the composition of fluid inclusions in marine halite and for the mineralogy of marine evaporites. The composition of fluid inclusions in primary marine halite reveals two major long-term cycles in the chemistry of seawater during the past 600 myr. The concentration of Mg^{2+}, Ca^{2+}, and SO_4^{2-} has varied quite dramatically. The Mg^{2+} concentration in seawater during most of the early Paleozoic and Jurassic to Cretaceous was as low as 30 to 40 mmol/kg H_2O; it reached maximum values $\geq$50 mmol/kg H_2O during the Late Neoproterozoic and Permian. The Ca^{2+} concentration in seawater during the Phanerozoic has reached maximum values two to three times greater than the concentration in seawater today (10.6 mmol/kg H_2O), whereas SO_4^{2-} concentrations may have been as low as 5 to 10 mmol/kg H_2O (a third to a fifth of the modern value) during the Jurassic and Early Paleozoic. The Mg^{2+}/Ca^{2+} ratio in seawater ranged from 1 to 1.5 during the early to middle Paleozoic and Jurassic-Cretaceous to a near-modern value of 5.2 during the Late Neoproterozoic and Permian. This change in seawater Mg^{2+}/Ca^{2+} ratio is consistent with the notion of alternating "calcite-aragonite seas" recorded in oölites and marine carbonate cements.

Several models have been proposed to explain the chemical evolution of seawater. These have invoked significant changes in one or more of the major geochemical processes that control the composition of seawater. The pattern and magnitude of the variations in the composition of seawater proposed in this study are similar to those proposed elsewhere that suggest that seawater fluxes through midocean ridges have played a major role in the evolution of seawater during the past 600 myr. Two Phanerozoic supercycles of the Earth's exogenic processes were recognized in the literature that are caused by mantle convection and plate activity. The composition of seawater has apparently undergone dramatic secular changes in phase with these supercycles and as a consequence of biological evolution. Analyses of fluid inclusions containing unevaporated seawater and a better understanding of the processes that affect the composition of seawater are needed to refine our understanding of the history of Phanerozoic seawater. *Copyright © 2002 Elsevier Science Ltd*

1. INTRODUCTION

Since Rubey's (1951) presidential address to the Geological Society of America, "The Geologic History of Sea Water—An Attempt to State the Problem," many efforts, ranging from equilibrium (Sillén, 1961, 1967) to steady-state (Mackenzie and Garrels, 1966; Maynard, 1976) to kinetic models (Broecker, 1971), have been made to constrain the composition of seawater during the Phanerozoic. In his presidential address to the Geochemical Society on "The Geologic History of Sea Water—An Attempt to Solve the Problem" and the first full-scale book on this subject, *The Chemical Evolution of the Atmosphere and Oceans*, Holland (1972, 1984) used the constancy of the mineral sequence during the early stages of marine evaporites to constrain the potential variability of the composition of Phanerozoic seawater. He was able to show that during this period, the concentration of the major constituents of seawater has probably varied by less than a factor of about two. Although this was an elegant approach, the limits that it set on the composition of Phanerozoic seawater were broad.

Following the pioneer work of Holser (1963), Lazar and Holland (1988) developed a technique for the precise determination of the concentration of all the major species as well as that of Br^- and Li^+ in brine inclusions $\geq$200 μm in diameter. This technique opened the way to a more direct approach to the study of the evolution of seawater by analyzing the composition of primary fluid inclusions in halite from marine evaporites. Horita et al. (1991) demonstrated that the composition of Permian seawater was similar to that of modern seawater. However, the composition of primary fluid inclusions in Jurassic, Silurian, and Devonian marine halite (Das et al., 1990; Land et al., 1995; Horita et al., 1996) turned out to be significantly different from that of brines generated by the evaporation of modern seawater. They were severely depleted in Mg^{2+} and SO_4^{2-}, and enriched in Ca^{2+}. This difference could be explained by the effects of dolomitization during the passage of seawater from the open ocean across large carbonate platforms to restricted evaporite basins. It was therefore possible to explain the composition of these inclusion fluids without calling on significant differences between the composition of modern seawater and the composition of seawater during the Silurian and Devonian. However, apparent lack of extensive contemporaneous dolomite in many evaporite basins casts doubt on the above interpretation.

It has been known for a long time that many Paleozoic and Mesozoic marine evaporites contain sylvite, carnallite, or both,

* Author to whom correspondence should be addressed (horitaj@ornl.gov).

and that they lack the $MgSO_4$-potash minerals, which precipitate during the evaporation of modern seawater. These "$MgSO_4$-poor" evaporites were considered "unusual" or "abnormal." Their composition was often ascribed to postdepositional alteration or to the evolution of brines under unusual conditions in restricted basins (Borchert and Muir, 1964; Braitsch, 1971; Hite, 1985; Ayora et al., 2001). However, it is the "normal" $MgSO_4$-rich marine evaporites that are the exception. They only account for ~5% of all known Phanerozoic evaporite deposits (Hardie, 1990; Herrmann, 1991). Increasingly, the data for the chemical composition of inclusions brines (Horita et al., 1996; Kovalevich et al., 1998; Lowenstein et al., 2001) has confirmed that brines in many Phanerozoic marine evaporite basins were indeed devoid of SO_4^{2-}. This observation, together with Sandberg's (1983) observation of long-term changes in the relative abundance of aragonite and calcite in oölites and marine carbonate cements, led Spencer and Hardie (1990) and Hardie (1996) to suggest that the composition of seawater has varied significantly during the Phanerozoic. They proposed that the composition of seawater changed in response to variations in the rate of seafloor spreading, which produced changes in the rate of seawater cycling through midocean ridges (MOR). Holland et al. (1996) pointed out several shortcomings in this model and showed that the effect of variations in spreading rates on global seawater composition is more modest than that proposed by Hardie (1996).

During the last several years, an increasing amount of information has been published on the composition of inclusion brines in halite deposits (Appendix), but disagreement continues regarding the relative importance of variations in the composition of seawater during the Phanerozoic (Kovalevich et al., 1998; Lowenstein et al., 1999; Timofeeff et al., 1999) and the alteration of seawater during its evaporation path, in restricted evaporite basins, or both (Holland et al., 1996; Holland and Zimmermann, 1998; Ayora et al., 2001). The availability of new, high-quality fluid inclusion data from many marine evaporites, acquired largely by our own efforts, prompts us to revisit the problem of the chemical evolution of seawater during the Phanerozoic.

2. MATERIALS AND METHODS

The use of the mineralogy of marine evaporites and of the composition of fluid inclusions in halite to reconstruct the chemical evolution of seawater is not free of difficulties: (1) Assumptions must be made in defining the degree of evaporation (DE)—that is, the ratio of the concentration of a conservative element in brines to that in the initial seawater. (2) Uncertainties are introduced by the precipitation of mineral phases (carbonates, gypsum/anhydrite, and halite) before and during halite precipitation. (3) Reactions of seawater with sediments en route to the evaporite basin (e.g., replacement of $CaCO_3$ by dolomite) must be taken into account. (4) Contribution of nonmarine solutions can affect the composition of waters in a basin. (5) Reactions with earlier evaporites (particularly potash minerals) and clastic/authigenic sediments can modify the composition of brines in an evaporite basin. (6) And postdepositional alteration due to diagenetic and burial metamorphic processes can affect the composition of inclusion brines in evaporite deposits.

Processes 1 and 2 above present fundamental problems associated with the use of the evaporite record to reconstruct the composition of seawater. They are discussed in detail in section 4. Difficulties 3 to 6 are related to hydrologic, sedimentologic, and diagenetic/metamorphic processes in evaporite basins, which can only be overcome by using a great deal of information regarding the geology, paleontology, sedimentology, and geochemistry of the evaporite basins. In general, the evaporite deposits that are most suitable for reconstructing the composition of the contemporaneous seawater are those that formed in deep basins devoid of carbonate platforms and without an input of clastic sediments. Bedded evaporites formed in stable sedimentary basins without postdepositional deformation are preferable to evaporites from tectonically active basins or salt domes. Basal halites deposited well before potash zones and close to an inlet of seawater to evaporite basins are preferred sources of samples. Primary, single-phase brine inclusions with negative crystal shapes in primary halite in which hoppers and chevrons are outlined by alternating bands of inclusion-rich and -free zones are preferable to two-phase, irregular inclusions in clear, diagenetic halite. It is difficult, if not impossible, to identify evaporite deposits that meet all these requirements. In this synthesis of large data sets of brine inclusions, our own and those available in the literature, we only consider halite from evaporite deposits whose Sr and S isotope signature indicates unequivocally that they are marine in origin. Whenever possible, halite of the same or similar geologic age from different evaporite basins is used to determine whether the composition of their inclusion fluids yields global rather than local/regional signatures. Only cubic, single-phase inclusions from growth bands within primary halite crystals have been used to constrain seawater compositions ("ch" in Appendix). Large, irregular inclusions in clear halite and two-phase inclusions suggestive of a diagenetic origin were eliminated from consideration.

During the last decade, several techniques have become available for the analysis of individual fluid inclusions in halite. The most precise (2 to 5% for major constituents) analyses are those obtained by microextraction followed by ion chromatography (Lazar and Holland, 1988) or by inductively coupled plasma mass spectrometry (ICP-MS; von Borstel et al., 2000). Both methods have the advantage that the concentration of Br^-, Li^+, and some other trace elements can also be determined, but with a precision of 3 to 15%. The measurement of Br^- is particularly useful for evaluating the DE_{Br} because Br^- is largely conservative during evaporation and precipitation and has a long residence time in the oceans (~100 myr; Holland, 1978). However, these techniques are only applicable to fluid inclusions with a diameter of >200 μm. The Petrichenko (1973) method permits the determination of K^+, Mg^{2+}, and SO_4^{2-} with a precision of ~20% by use of microextraction and wet chemical methods of analysis. However, these ions are usually not determined in brines from the same inclusion. In many instances, the origin of samples and the primary nature of the fluid inclusions are poorly documented (e.g., Kovalevich et al., 1998). Such data are therefore not suitable for defining the chemical evolution of seawater. Ayora and Fontarnau (1990) have pioneered a cryo-SEM-EDS technique for measuring Na^+, K^+, Mg^{2+}, Ca^{2+}, SO_4^{2-}, and Cl^- in fluid inclusions <250 μm in diameter. The uncertainty in their measurements is 10 to 20% (see also Timofeeff et al., 2000). More recently, fluid inclusions as small as 20 μm in diameter have been selectively opened with an ultraviolet laser, and the brines have been analyzed for Mg^{2+}, Ca^{2+}, K^+, and a variety of trace elements by ICP-MS (Shepherd and Chenery, 1995; Shepherd et al., 1998). Although LA-ICP-MS can provide high-precision values of element ratios, the volume of the inclusions cannot be determined; hence, these analyses only define the relative concentrations of elements.

Data for the chemistry of inclusion brines were first presented in Jänecke units and diagrams (Braitsch, 1971; Usdowski and Dietzel, 1998) (Appendix and Figs. 1 to 4). Jänecke diagrams are useful for showing the major features of the chemistry of NaCl-saturated brines, particularly the differences between SO_4-rich and Ca-Cl type brines. Saturation indexes for potash minerals (sylvite, carnallite, $MgSO_4$ minerals, etc.) were calculated on the basis of the Harvie et al. (1984) model, and data for inclusion brines that are saturated with respect to these late-stage minerals were discarded. Geochemical screening as proposed by Zimmermann (2001) has been applied to identify primary fluid inclusions that contain evaporated seawater before potash mineral precipitation and without an overprint of evaporite recycling ("sw" in Appendix). In the Jänecke-diagram of Mg-2K-SO_4 or Mg-Ca-2K, the position of seawater does not change during halite precipitation after the precipitation of carbonates and gypsum/anhydrite until the onset of the precipitation of potash and $MgSO_4$-bearing minerals. The precipitation and dissolution of complex $CaSO_4$ minerals such as polyhalite and glauberite during the halite facies change Jänecke values only modestly (Eugster et al., 1980).

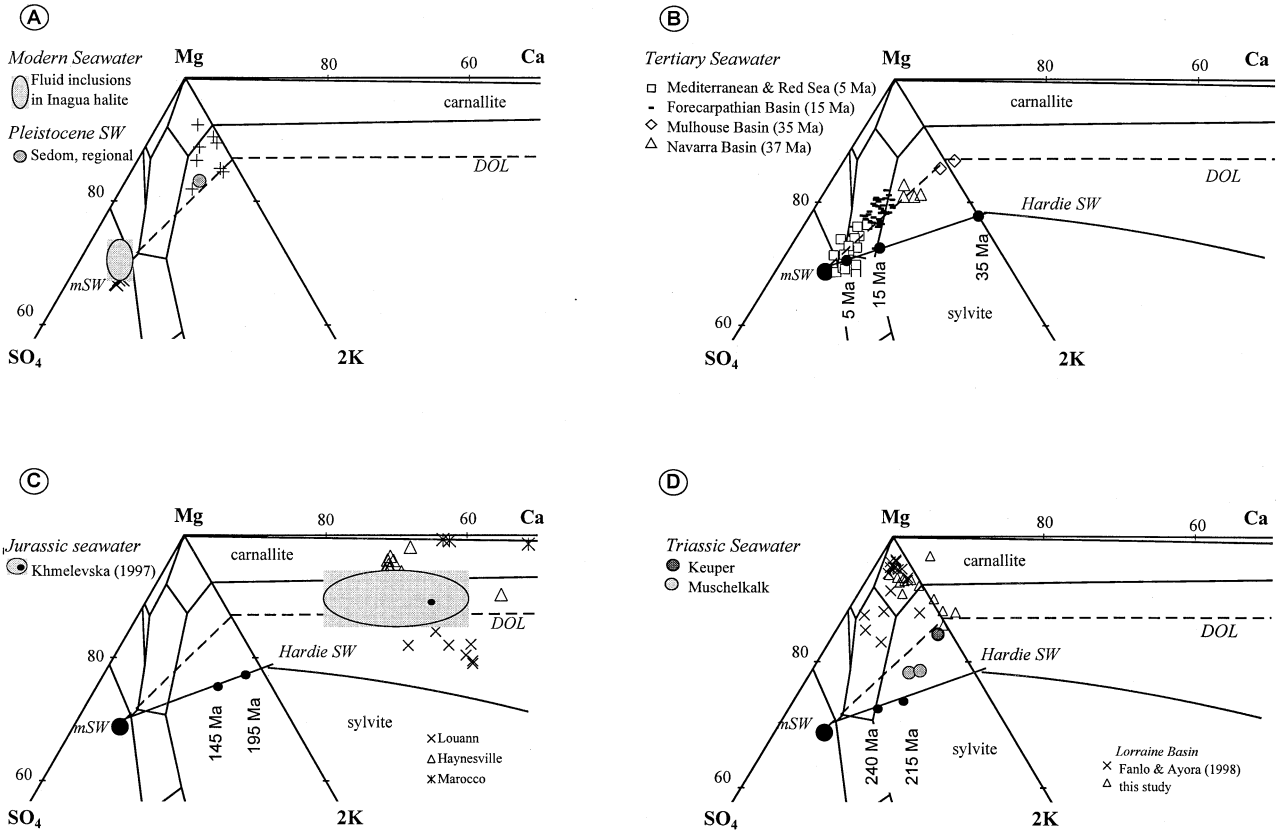

Fig. 1. Compositions of fluid inclusions (mol%) from Cenozoic and Mesozoic marine halite in the Mg-2K-SO_4 and Mg-Ca-2K Jänecke diagrams at 25°C. (A) Modern and Quaternary. +, fluid inclusions that are not simply evaporated seawater before the potash facies. (B) Tertiary. (C) Jurassic. (D) Triassic. mSW = modern seawater at the halite facies; DOL = predicted chemistry of seawater affected by the dolomitization of limestones during evaporative concentration; Hardie SW = predicted seawater chemistry caused by variations in seafloor spreading rates according to Hardie (1996). Stability fields of solid phases are labeled. For sample description and analytical data, see Appendix.

3. EVALUATION OF DATA SETS

3.1. Modern and Cenozoic

Von Borstel et al. (2000) have confirmed that the composition of brine inclusions from the solar salt works on Great Inagua Island plot on the projection point of unevaporated modern seawater in the Jänecke diagram at 25°C (Fig. 1A). Timofeeff et al. (2001) obtained similar results for the major species Na^+, K^+, Mg^{2+}, Cl^-, and SO_4^{2-} in inclusion brines from modern halite taken from a supratidal sabkha in Baja California, which have undergone repeated cycles of flooding, dissolution, and precipitation of evaporite minerals. These results show that inclusion brines in marine evaporites faithfully record the composition of evaporated modern seawater. However, brines trapped within fluid inclusions may not be simply evaporated seawater. Our analyses of fluid inclusions from five samples of marine halite of the Plio-Pleistocene (1 to 2 Ma) Sedom Formation in the Dead Sea rift valley in Israel (Zak, 1997) show that the brines in this basin were depleted in Mg^{2+} and SO_4^{2-} relative to modern seawater (Fig. 1A and Appendix). The isotopic composition of Sr in carbonates, gypsum/anhydrite, and halite in this formation (Stein et al., 2000) clearly indicates that the brines in the Dead Sea rift valley have been modified by interaction (dolomitization) with Late Cretaceous carbonates. This observation underscores the importance of isotopic data for the interpretation of fluid inclusion analyses.

An extensive set of fluid inclusion analyses is now available for Tertiary marine halites. The set includes analyses of the Late Miocene evaporites of the Red Sea and the Mediterranean (Lazar and Holland, 1988; Ayora et al., 1994a; Garçia-Veigas et al., 1995; Kovalevich et al., 1997; Zimmermann; 2000b; Lazar and Holland, personal communication), the Middle Miocene evaporites of the Carpathian Foredeep Basin (Galamay et al., 1997; Galamay and Karoli, 1997; Garçia-Veigas et al., 1997; Kovalevich and Petrichenko, 1997; Shaidetska, 1997; Kovalevich et al., 1998; Bukowski et al., 2000) and the Oligo/Eocene evaporites of the Mulhouse and Navarra Basins (Canals et al., 1993; Ayora et al., 1994b). Zimmermann (2000a) reviewed these data and showed that during the last 40 myr, the concentration of Mg^{2+} in seawater gradually increased from ~37 to 55 mmol/kg H_2O (Fig. 1B and Appendix).

3.2. Mesozoic

On the basis of cryo-SEM-EDS fluid inclusion analyses in chevron halite of the Congo Basin in Africa, the Sergipe Basin in Brazil, and the Khorat Plateau in Thailand and Laos, Timofeeff et al. (1999) estimate that compared with modern

seawater Cretaceous seawater was considerably enriched in Ca^{2+} and depleted in Mg^{2+} by 30 to 40%. No details concerning their analytical results for individual fluid inclusions are available. The Cretaceous evaporites of Africa and South America are related to the opening of the Atlantic (Belmonte et al., 1965; Wardlaw, 1972). These deposits and the Thailand evaporites (Hite and Japakasetr, 1979; El Tabakh et al., 1999) do not contain marine carbonates at the base of the sequence but include tachyhydrite, sylvite, and carnallite. Hardie (1990) and Garrett (1996) proposed a nonmarine origin for these evaporites or a considerable hydrothermal contribution to the evaporite basins. However, the mineralogy of these "unusual" Cretaceous evaporites can be explained as primary precipitates from evaporated seawater of the composition proposed by Timofeeff et al. (1999).

Land et al. (1995) have reported analyses of 12 fluid inclusions in three samples of chevron halite from the Middle-Late Jurassic Louann Formation of the Gulf Coast (Fig. 1C and Appendix). Our new analyses include 14 inclusion brines in three halite samples from the overlying Late Jurassic Haynesville Formation, which were also obtained from the Champion-Klepac 1 well in Alabama, and five fluid inclusions from the Early Jurassic evaporites offshore from Morocco (DSDP site 546; see Clement and Holser, 1988). Saturation calculations with the Harvie et al. (1984) model show that many of these inclusion brines are saturated with respect to sylvite, carnallite, or both, suggesting that much of the information regarding the composition of the original seawater has been lost. Khmelevska (1997) studied the composition of primary fluid inclusions in chevron halite of the Kimmeridgian evaporites of the Ukraine by using the Petrichenko method. She tabulated only an average composition for all of the primary inclusions with a considerable range of data (Fig. 1C). This average composition represents brines well before the potash facies with average Jänecke units of 58.3 mol% for Mg, 8.5 mol% for 2K, and 33.2 mol% for Ca. The analyses of the fluid inclusions from the Gulf Coast Basin and Ukraine overlap. The Gulf of Mexico Basin is devoid of massive carbonate deposits of Louann age (Tew et al., 1991). It is therefore unlikely that the inclusion brines in halite from the Louann (and Haynesville) were altered by the dolomitization of limestone en route from the open sea to the evaporite basin. Altogether, this suggests strongly that the composition of Cretaceous and Jurassic seawater was quite different from that of modern seawater.

Kovalevich et al. (1998) and Kovalevich and Hauber (2000) reported the average composition of brine inclusions from the Early Triassic Röt evaporites (Buntsandstein) in the Netherlands and in Poland. These evaporites are associated with nonmarine clastic sediments. Br^- analyses (Holser and Wilgus, 1981) and our isotopic analyses of S and Sr do not allow an unequivocal assignment of a marine or continental origin to these deposits. The Röt evaporites have been variously interpreted as reworked salt of the underlying Permian Zechstein evaporites and desiccation products of largely continental waters. Their origin is so uncertain, that they have not been included in this compilation.

Shallow marine carbonates and marginal marine evaporites of the Middle Triassic Muschelkalk Basin were deposited in an elongated gulf stretching from northern Germany to southern France. In Switzerland the thickness of this unequivocally marine halite sequence reaches 100 m, and initial sedimentary features are occasionally preserved. S and Sr isotopic composition suggest a marine origin (Holser, personal communication). Kovalevich and Hauber (2000) analyzed primary fluid inclusions in two samples of chevron halite from two wells in the Rheinfelden area by using the Petrichenko (1973) method. In the Jänecke diagram, their average compositions plot in the stability field of sylvite between the seawater composition predicted by Hardie (1996) and the path predicted for seawater affected by the dolomitization of limestones (DOL in Fig. 1D). They appear to contain evaporated seawater before potash mineral precipitation.

Fanlo and Ayora (1998) analyzed primary fluid inclusions in 19 chevron halite samples from the Late Triassic (Early Carnian, Keuper) evaporites in the Lorraine Basin in France via the cryo-SEM-EDS technique. Most of the inclusion data plot in the stability field of either kainite or carnallite (Fig. 1D), although they are clearly not saturated with these potash minerals. In this study, we extracted 15 fluid inclusions from three chevron halite samples from the Varangeville salt mine in the same basin. Four of 15 inclusion fluids are $MgSO_4$ free and contain small amounts of $CaCl_2$. They are similar to the brines studied by Fanlo and Ayora (1998). However, saturation indexes based on the Harvie et al. (1984) model indicate that they are strongly evaporated and saturated with respect to sylvite or carnallite. Few data from fluid inclusions in Triassic halites are suitable for constraining the composition of seawater, and they scatter considerably (Fig. 1D). However, they definitely plot in the Mg-2K-SO_4 part of the Jänecke diagram.

3.3. Paleozoic

Permian marine evaporites, which are widespread in North America (Guadelupian and Ochoan ages) and in Europe (Zechstein age), are among the best-studied evaporite deposits. The entire sequence of Zechstein evaporites was deposited in less than 7 myr (Menning, 1995). The Z1 and Z2 formations of the German Zechstein evaporites contain $MgSO_4$ minerals such as langbeinite, kieserite, and polyhalite, whereas Z3 does not. The Z3-sylvinites of the Hannover district are clearly alteration products of earlier carnallitic rocks (Peters, 1988), and our analyses of inclusion fluids from the time-equivalent Boulby halite in England (Fig. 2D and Appendix) suggest a similar origin for this unit. Herrmann et al. (1997) investigated primary fluid inclusions in the Allertalgraben Z3 halite. The compositions of all of the fluid inclusions plot in the stability fields of kainite, sylvite, or carnallite with average Jänecke units of 78.5 $\pm$ 1.6 mol% for Mg, 8.0 $\pm$ 1.2 mol% for 2K, 13.5 $\pm$ 1.0 mol% for SO_4 (n = 9, Appendix; Fig. 2D). By means of the Petrichenko (1973) method, Peryt and Kovalevich (1996) analyzed primary fluid inclusions in 20 samples of chevron halite from the basal Z1 formation (Fig. 2B and Appendix). Many fluid inclusions contain evaporated seawater with average Jänecke values of 77.3 $\pm$ 2.2 mol% for Mg, 8.2 $\pm$ 0.9 mol% for 2K, 14.5 $\pm$ 1.9 mol% for SO_4 (n = 8) (Fig. 2B). Thus, the compositions of seawater in the Z1 of Poland and the Z3 of Germany overlap (Fig. 2A).

A large number of analyses of fluid inclusions from primary bedded halite are available for the Ochoan Salado Formation in the Delaware and Palo Duro basins of North America (Stein

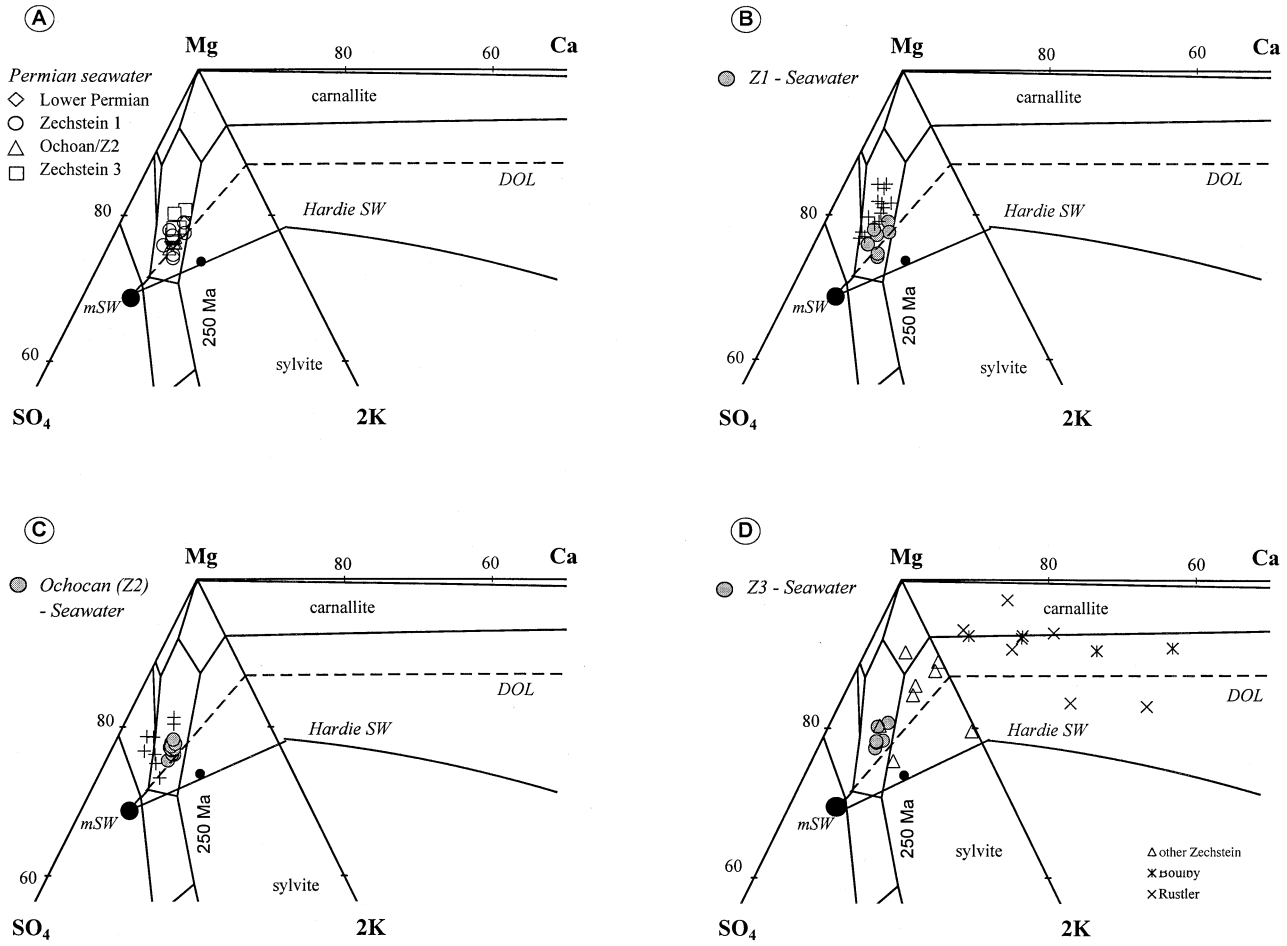

Fig. 2. Compositions of fluid inclusions (mol%) from Permian marine halite in the Mg-2K-SO_4 and Mg-Ca-2K Jänecke diagrams at 25°C. (A) Lower and Upper Permian primary fluid inclusions of evaporated seawater before potash facies. (B) Zechstein 1. (C) Ochoan. (D) Zechstein 3 and Rustler Formation. mSW = modern seawater at the halite facies; DOL = predicted chemistry of seawater affected by the dolomitization of limestones during evaporative concentration; Hardie SW = predicted seawater chemistry caused by variations in seafloor spreading rates according to Hardie (1996). Stability fields of solid phases are labeled. For sample description and analytical data, see Appendix.

and Krumhansl, 1988; Bein et al., 1991; Horita et al., 1991; Lowenstein et al., 1999), which are time equivalents of Zechstein 2. Unfortunately, the data sets of Stein and Krumhansl (1988) and Bein et al. (1991) are not useful because the fluid inclusions are clearly not primary in origin. The results of Bein et al. (1991) also show a large degree of scatter, presumably due to varying degrees of reaction with minerals on the associated carbonate platform. Horita et al. (1991) analyzed 24 primary fluid inclusions extracted from two samples of chevron halite from the Delaware Basin. The calculated saturation indexes suggest that most of these inclusions are evaporated seawater before the beginning of the potash facies and that they were not affected by the dissolution of potash minerals. In the Jänecke diagram, they plot in the stability field of kainite with average Jänecke units of 76.8 ± 1.2 mol% for Mg, 8.0 ± 0.4 mol% for 2K, 15.2 ± 1.2 mol% for SO_4 (n = 18, Appendix) (gray circles, Fig. 2C). The composition of seawater in the Ochoan Delaware Basin of North America and in the European Zechstein Basin overlaps (Fig. 2A). Horita et al. (1991) also extracted and analyzed 14 fluid inclusions from marine halite of the Early Permian (Leonardian) Wellington Formation in the Kansas Basin. Their Jänecke units of 79.1 mol% for Mg, 8.6 mol% for 2K, and 12.4 mol% for SO_4 (Appendix) are consistent with the inferred compositional range of Upper Permian seawater. ESEM analyses of primary fluid inclusions from chevron halite in the Salado and San Andres formations of the Delaware and Palo Duro Basins by Lowenstein et al. (1999) confirm these results. All of the data indicate Jänecke units of 77.8 ± 1.2 mol% for Mg, 8.2 ± 0.4 mol% for 2K, and 14.0 ± 1.2 mol% for SO_4 for Permian seawater, which is close to those of modern seawater.

Petrichenko (1973) and Petrychenko et al. (in press) analyzed fluid inclusions from 15 samples of Carboniferous Viséan evaporites (Penobsquis Salt Member of the Cassidy Lake Formation) in the Moncton Subbasin, New Brunswick, Canada via the Petrichenko (1973) method. However, according to Petrychenko et al. (in press), the beginning and the end of the deposition of the Windsor Group evaporite sequence was strongly influenced by waters of nonmarine origin. Hence, this deposit is not suitable for determining the composition of Carboniferous seawater.

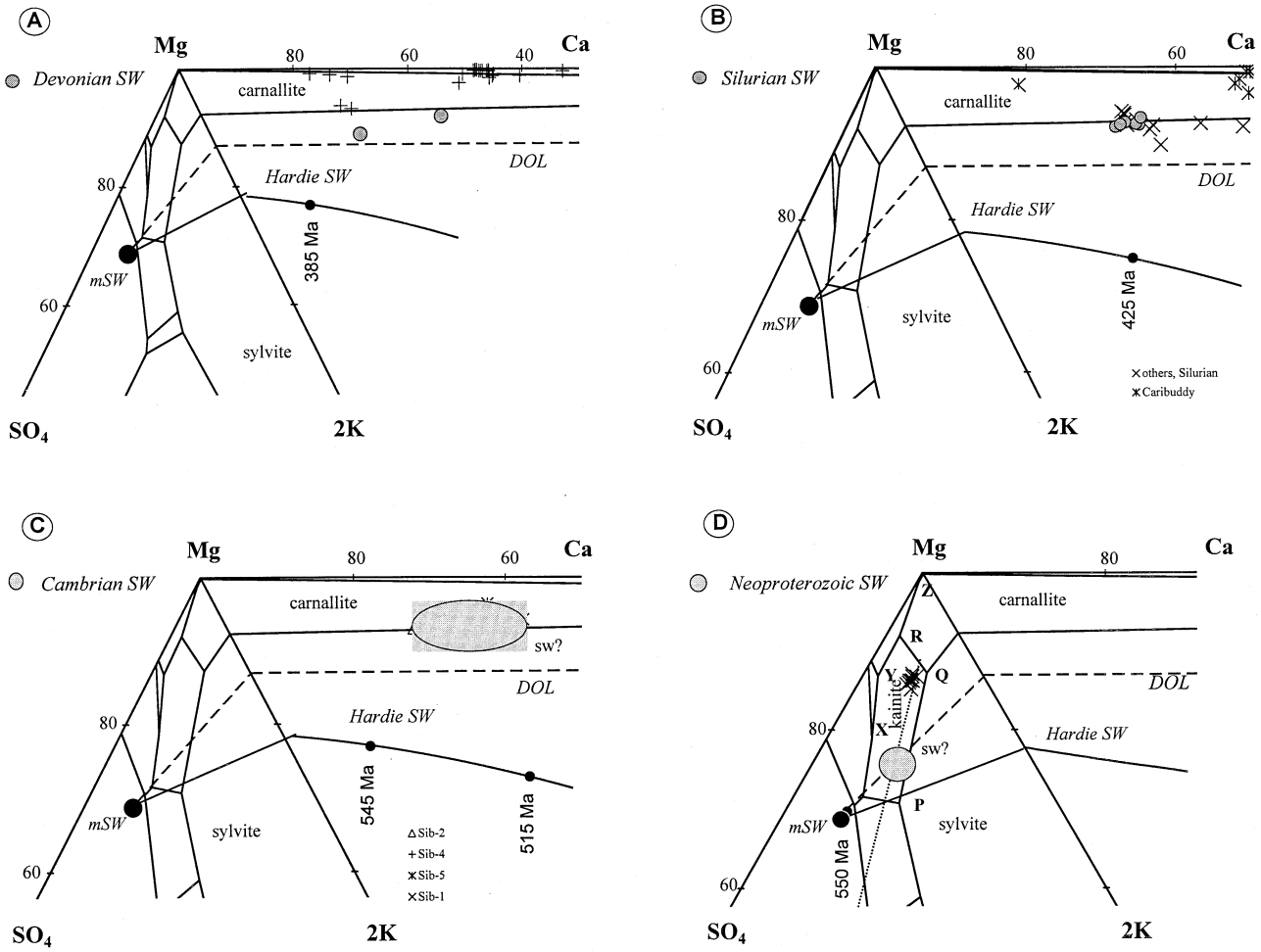

Fig. 3. Compositions of fluid inclusions (mol%) from Paleozoic marine halite in the Mg-2K-SO_4 and Mg-Ca-2K Jänecke diagrams at 25°C. (A) Devonian. (B) Silurian. (C) Early Cambrian. (D) Late Neoproterozoic. mSW = modern seawater at the halite facies; DOL = predicted chemistry of seawater affected by the dolomitization of limestones during evaporative concentration; Hardie SW = predicted seawater chemistry caused by variations in seafloor spreading rates according to Hardie (1996). Stability fields of solid phases are labeled. P, Q, R, X, Y, and Z designate invariant brine compositions (Usdowski and Dietzel, 1998). For sample description and analytical data, see the Appendix.

Horita et al. (1996) investigated inclusion brines in marine halite from the Middle Devonian (377 to 386 Ma) Elk Point Group (Prairie Formation) of the Saskatchewan Subbasin in Canada via the Lazar and Holland (1988) technique. In a total of 26 fluid inclusions in seven halite samples from three sites in the southern part of the Saskatchewan Subbasin, only the fluid inclusions in the well samples (AW46-49, Appendix) were extracted from growth bands of cloudy chevron halite. The inclusion brines plot in the stability fields of sylvite and carnallite in the $CaCl_2$-rich and $MgSO_4$-free part of the diagram (Mg-Ca-2K, Fig. 3A). Many fluids extracted from halite in the IMC mine are extremely concentrated and saturated with respect to carnallite. Only chevron halite AW49-F26 from Bredenbury and AW46 from Lanigan seem to contain primary fluid inclusions of evaporated seawater before reaching the potash facies. Kovalevich et al. (1998) reported average compositions of inclusion brines from two Middle and seven Late Devonian evaporite deposits from the former Soviet Union. These are similar to those of the Middle Devonian Prairie Formation in Western Canada.

Das et al. (1990) reported the composition of 18 fluid inclusions in four marine halite samples from unit F of the Late Silurian Salina Group of the Michigan Basin. The samples of bedded halite contain abundant chevron structures, and the extracted fluid inclusions were located next to these growth bands ("ch" in Appendix). Other fluids were extracted from single-phase inclusions that were randomly distributed in pod halite. The calculations of saturation indexes demonstrate that the brines in the halites from the Michigan Basin were not saturated with the respect to sylvite or carnallite, and that they can be used to constrain the composition of Late Silurian seawater. However, the analyses of inclusion fluids in these samples need to be treated with some caution because the brine compositions seem to have been affected by the dissolution and precipitation of halite. This might have reduced the Br concentration of the brines. The brine compositions plot close to the

boundary between the stability fields of sylvite and carnallite in the $CaCl_2$-rich and $MgSO_4$-free part of the Jänecke diagram (Mg-Ca-2K, open circles in Fig. 3B). In this study, we extracted several individual inclusions from a halite sample of the Late Ordovician-Early Silurian Mallowa Salt of the Carribuddy Group in the Canning Basin of Western Australia (Cathro et al., 1992). Saturation indexes indicate saturation with carnallite for all the Carribuddy halite inclusions. Overall, the data suggest that the composition of Silurian seawater was significantly different from that of modern seawater.

We studied 15 fluid inclusions (Appendix) in four samples of white cloudy halite and gray halite with few chevrons from the Early Cambrian evaporites of Eastern Siberia. The exact location of our samples is not known, and the geology and sedimentology of the evaporites, which were deposited on a Precambrian carbonate sequence, are not well described (Grishina et al., 1992). A few inclusions from growth bands were extracted and analyzed via the Lazar and Holland (1988) technique. Calculations of saturation indexes indicate that many inclusions are saturated with respect to sylvite or carnallite. Only a few fluids in sample Sib-4 may contain evaporated seawater before the potash facies. Their average composition is 57.9 ± 4.2 mol% for Mg, 5.9 ± 0.5 mol% for 2K, and 36.2 ± 3.7 mol% for Ca ($n = 5$) in the $CaCl_2$-rich and $MgSO_4$-free part of the Jänecke diagram (Mg-Ca-2K, Fig. 3C). If these inclusions represent evaporated Early Cambrian seawater, then seawater at that time was depleted in Mg^{2+} and enriched in Ca^{2+} relative to modern seawater.

3.4. Late Proterozoic

In the Late Neoproterozoic, a marine carbonate-evaporitic facies spread across much of the Pangea landmass from the Indian subcontinent (Rajasthan, Salt Range in Pakistan; Jones, 1970; Das Gupta et al., 1988; Banerjee et al., 1998; Banerjee and Mazumdar, 1999), through South Yemen, Oman (Ara-Formation; Gorin et al., 1982; Mattes and Morris, 1990), and Saudi Arabia to Iran (Hormuz Series, carbonate platform north of the Zagros mountains; Folle and Beutel, 2000). The Hanseran Evaporite Group in Rajasthan contains $MgSO_4$ minerals (polyhalite, kainite, langbeinite) together with sylvite and carnallite. Sizable accumulations of $MgSO_4$ salts are also reported from the Salt Range evaporites in Pakistan (Jones, 1970).

We have analyzed nine fluid inclusions (Appendix) from patches of chevrons in a halite sample from the Ara Formation in Oman (Gorin et al., 1982; Mattes and Morris, 1990) by using the technique developed by Lazar and Holland (1988). In the Jänecke diagram they plot in a narrow field close to the boundary between the stability fields of kainite and sylvite (Fig. 3D). All of them are saturated with respect to kainite and carnallite. Despite the advanced evaporation of the brines, the composition of the primary fluid inclusions in halite from the Ara Formation together with the mineralogy of potash salts from the Indian Nagaur-Ganganagar and Pakistan Salt Range evaporite basins can set some limits on the chemistry of Neoproterozoic seawater. Like Permian seawater, it was comparatively rich in Mg^{2+} and SO_4^{2-}.

4. RECONSTRUCTION OF THE COMPOSITION OF PHANEROZOIC SEAWATER

The above examination and evaluation of the available inclusion data show that during the Phanerozoic the composition of brines in marine evaporite deposits has experienced several swings between being $MgSO_4$ rich and $CaCl_2$ rich (Fig. 4). Kovalevich et al. (1998) reached a similar conclusion on the basis of their own sets of brine inclusions from halite deposits in large part from Europe and the former Soviet Union. It is therefore likely that the dramatic swings in brine chemistry largely reflect changes in the composition of seawater rather than the effects of local or regional processes.

The composition of fluid inclusions in halite from marine evaporites in Figure 4 can now be used—within limits—to define the chemical evolution of seawater during the Phanerozoic. Fluid inclusions that show the effects of local/regional hydrologic, sedimentologic, and diagenetic processes (processes 3 to 6 discussed in section 2), have been excluded from consideration. The evaporation of seawater increased the concentration of all the dissolved species, and the precipitation of carbonates and gypsum/anhydrite clearly influenced the concentration of Ca^{2+}, HCO_3^-, and SO_4^{2-} in all of the inclusion brines. It is also likely that dolomitization influenced the Mg^{2+} content of some inclusion brines.

Because the concentration of K^+, Mg^{2+}, Ca^{2+}, and SO_4^{2-} in inclusion brines from marine halite deposits has been affected by evaporative concentration, by the precipitation of carbonates and gypsum/anhydrite, and by dolomitization, the concentration m_i (mmol/kg H_2O) of these elements in the initial seawater is

$$m(K^+)/DE = m(K^+)_i \quad (1)$$

$$m(Mg^{2+})/DE = m(Mg^{2+})_i - y \quad (2)$$

$$m(Ca^{2+})/DE = m(Ca^{2+})_i + y - x \quad (3)$$

$$m(SO_4^{2-})/DE = m(SO_4^{2-})_i - x \quad (4)$$

where DE is the degree of evaporation (see section 2), x is the quantity of $CaSO_4$ in mmol/kg H_2O precipitated from the evaporating seawater, and y is the quantity of dolomite in mmol/kg H_2O generated by the replacement of $CaCO_3$ by in-basin dolomitization. The Ca^{2+} concentration of the inclusion fluids has also been modified by the precipitation of $CaCO_3$. Today, the loss of Ca^{2+} due to $CaCO_3$ precipitation amounts to only ~10% of the quantity initially present in seawater. During the course of the Phanerozoic, the loss of Ca^{2+} due to $CaCO_3$ precipitation was probably even smaller and can, to a first approximation, be neglected. With the microextraction/ion chromatography technique of Lazar and Holland (1988), the concentration of Br^- in inclusion brines can be determined. These concentrations were used to calculate DE of the inclusion fluids, assuming that the Br^- concentration of seawater has not changed significantly during the Phanerozoic. This seems reasonable because Br^- has a residence time of ~100 myr. The Br^- and K^+ data for inclusion brines from halite deposits that were not affected by the recycling of potash minerals suggest that the concentration of K^+ in seawater has changed little during the Phanerozoic (Table 1 and Fig. 5). In the absence of Br^- data with the Petrichenko and SEM-EDS

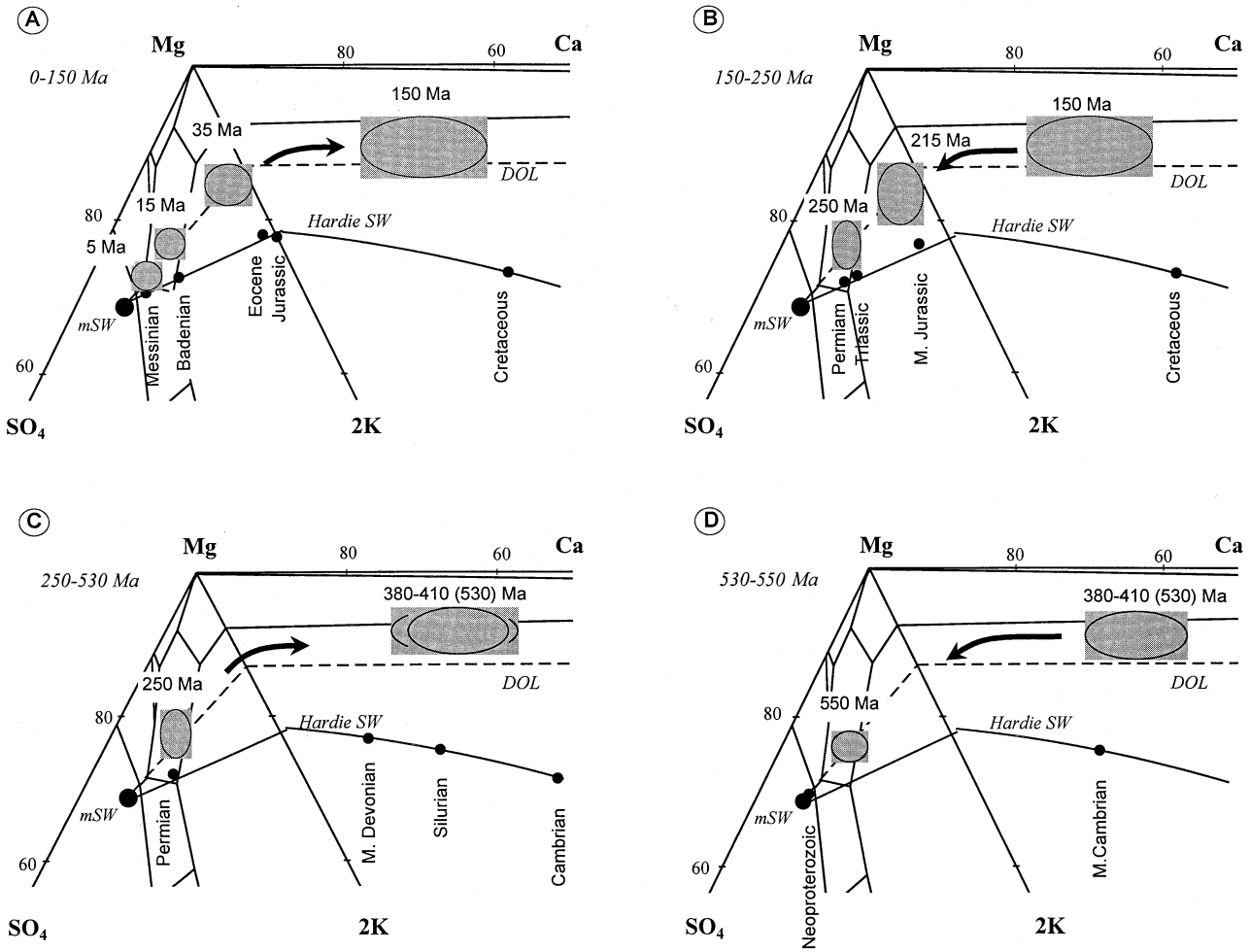

Fig. 4. Composition of Phanerozoic seawater (mol%) in the Mg-2K-SO_4 and Mg-Ca-2K Jänecke diagrams at 25°C estimated from primary fluid inclusions in marine halite (A) For 0 to 150 Ma. (B) For 150 to 250 Ma. (C) For 250 to 390/410 (/530) Ma. (D) For 390/410 (/530) to 550 Ma. mSW = modern seawater at the halite facies; DOL = predicted chemistry of seawater affected by the dolomitization of limestones during evaporative concentration; Hardie SW = predicted seawater chemistry caused by variations in seafloor spreading rates according to Hardie (1996). Stability fields of solid phases are labeled.

methods, we have used the concentration of K^+ in their inclusion brines to estimate DE, assuming that the concentration of this element was the same as that of modern seawater (Fig. 5).

Table 1. The concentration of K^+ (mmol/kg H_2O) in seawater during the Phanerozoic on the basis of the composition of selected fluid inclusions in marine evaporites.

Time	Age (Ma)	$m(K^+)_i$
Modern seawater	0	10.6
Messinian	5	10.8 ± 0.4
Upper Triassic	230	9.3
Upper Permian	250	10.9 ± 1.1
Lower Permian	270	10.3
Middle Devonian	380	10.1
Upper Silurian	420	11.5 ± 0.2
Late Proterozoic	550	≥9

4.1. Cenozoic

No or little dolomite was produced by in-basin replacement of $CaCO_3$ in the Tertiary halite deposits listed in the Appendix (see also Zimmermann, 2000a). Thus, the Mg^{2+} concentration in Tertiary seawater can be calculated from the measured Mg^{2+}/Br^- or Mg^{2+}/K^+ ratios of the inclusion brines, assuming constancy of $m(K^+)_i$ and $m(Br^-)_i$ during the past 40 myr (Table 2). The Mg^{2+} concentration in seawater has apparently increased from 35 to 38 mmol/kg H_2O during the early Tertiary to 43 to 48 mmol/kg H_2O during the Miocene, to 55 mmol/kg H_2O in the present ocean (Fig. 6).

The solution of Eqns. 3 and 4 to obtain the value of $m(Ca^{2+})_i$ and $m(SO_4^{2-})_i$ requires an additional constraint. The product $m(Ca^{2+})_i \cdot m(SO_4^{2-})_i$ is one of these. Its value is a measure of the degree of saturation of seawater with respect to anhydrite, $CaSO_4$. The present value of this product is 305 (mmol/kg $H_2O)^2$. Seawater at 25°C becomes saturated with respect to gypsum at a DE of 3.8 (McCaffrey et al., 1987). This is

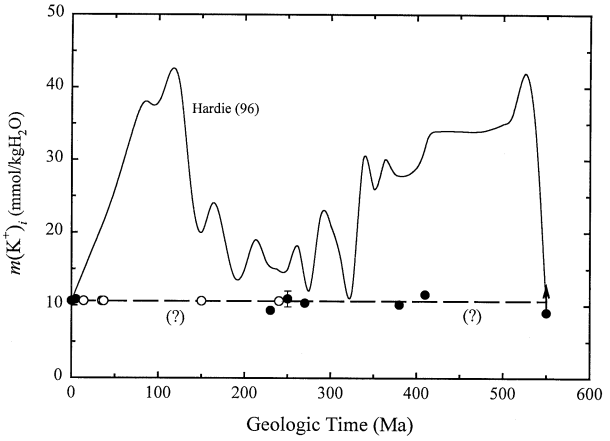

Fig. 5. Concentration of K^+ in seawater during the Phanerozoic based on analyses of fluid inclusions in marine halite (solid circles = analyses; open circles = assumption) compared with the variation predicted by Hardie (1996). For inclusion data, see Table 2.

considerably smaller than 1700 (mmol/kg H_2O)^2, the value of the product in seawater that is saturated with respect to gypsum at 25°C. It is considerably larger than 23 (mmol/kg H_2O)^2, the value of the product at which anhydrite precipitation at 25°C begins at the same DE as halite (Holland, 1984; Horita et al., 1991). If the product was larger than 305 (mmol/kg H_2O)^2 in the past, the precipitation of gypsum began at a smaller DE. Conversely, if the product was smaller than today, the precipitation of gypsum began at a larger DE.

It is intriguing to explore the consequences of the proposition that the product $m(Ca^{2+})_i \cdot m(SO_4^{2-})_i$ has remained essentially constant during the Cenozoic. With this assumption Eqns. 3 and 4 can be solved, and the values of $m(Ca^{2+})_i$ and $m(SO_4^{2-})_i$ can be calculated from the analyses of fluid inclusions in the Tertiary marine evaporites that have been studied to date. The validity of the results can be checked by comparing the trend of the $m(Mg^{2+})_i/m(Ca^{2+})_i$ ratio based on these calculations with the trend provided by independent estimate of the $m(Mg^{2+})_i/m(Ca^{2+})_i$ ratio in Tertiary seawater. There are two imprecise estimates of this ratio during the early Tertiary. One is based on the switch of the oceans from "aragonite" to "calcite" seas. Sandberg (1983, 1985) observed long-term variations in the relative abundance of aragonite and calcite in oölites and marine carbonate cements. He suggested that the oceans were "aragonite seas" between 0 and 57 ± 10 Ma, between 180 and 340 Ma, and before 550 Ma, but that they were "calcite seas" between 57 ± 10 Ma and 180 Ma, and between 340 and 550 Ma. Morse et al. (1997) demonstrated that the mineralogy of marine carbonates is a function of temperature and of the $m(Mg^{2+})_i/m(Ca^{2+})_i$ ratio of seawater. At 15°C, calcite precipitates from artificial seawater with a molar $m(Mg^{2+})_i/m(Ca^{2+})_i$ ratio ≤ 2, whereas aragonite precipitates from artificial seawater with a molar $m(Mg^{2+})_i/m(Ca^{2+})_i$ ratio ≥ 2. At 20°C, the threshold value of the $m(Mg^{2+})_i/m(Ca^{2+})_i$ ratio is 1.2. It seems reasonable, therefore, to use a threshold value of 1.5 ± 0.5 for the $m(Mg^{2+})_i/m(Ca^{2+})_i$ ratio in seawater at which calcite has switched to aragonite in oölites and marine cements during the Phanerozoic. Füchtbauer and Hardie (1976) reported similar experimental results. Figure 7 shows the value of $m(Mg^{2+})_i/m(Ca^{2+})_i$ derived from fluid inclusion data on the assumption that the product $m(Ca^{2+})_i \cdot m(SO_4^{2-})_i$ remained constant during the Tertiary, and the $m(Mg^{2+})_i/m(Ca^{2+})_i$ ratio indicated by the early Tertiary switch from "aragonite" to "calcite" seas. The two estimate of the course of $m(Mg^{2+})_i/m(Ca^{2+})_i$ ratio agree within their rather imprecise limits.

Changes in the Mg content of benthic foraminiferal calcite offer a second method of calculating the course of $m(Mg^{2+})_i/m(Ca^{2+})_i$ ratio in seawater during the Cenozoic. The Mg/Ca ratio of benthic foraminifera varies linearly with the $m(Mg^{2+})_i/m(Ca^{2+})_i$ ratio of seawater and exponentially with the temperature at which they grow. The only available data for the Mg content of a long-lived benthic foraminiferal species are those of Lear et al. (2000) for *Oridorsalis umbonatus*. If the $\delta^{18}O$ record of marine calcite is used to reconstruct the temperature during the Eocene, and if the coefficient of the temperature in the exponential term is set equal to 0.10 for *O. umbonatus* as suggested by Lear et al. (2000), the $m(Mg^{2+})_i/m(Ca^{2+})_i$ ratio of seawater 50 ± 2 myr ago is calculated to be 2.1 ± 0.7. The large uncertainty in the $m(Mg^{2+})_i/m(Ca^{2+})_i$ ratio computed in this fashion is due in part to the uncertainty in the assumed temperature, in part to uncertainties in the coefficient of the temperature, and in part to potential changes in the Mg content of the foraminifera during diagenesis. More data for other foraminifera are needed, but the general agreement between the estimate of the $m(Mg^{2+})_i/m(Ca^{2+})_i$ ratio based on this approach and that based on the "aragonite-calcite" transition is encouraging (Fig. 7). Both sets of observations are consistent with those obtained from inclusion brines of the Tertiary halites under the assumption of a constant value for the product $m(Ca^{2+})_i \cdot m(SO_4^{2-})_i$ during the Cenozoic. On this basis it follows that in the early Tertiary $m(Ca^{2+})_i$ was 16 to 17 mmol/kg H_2O and that it has decreased gradually to its present value of 10.6 mmol/kg H_2O (Fig. 8). The estimated concentration of SO_4^{2-} increased from 17 to 19 mmol/kg H_2O during the Oligocene and Eocene to its present value of 29 mmol/kg H_2O (Fig. 9). Varying the product $m(Ca^{2+})_i \cdot m(SO_4^{2-})_i$ from half to 1.5 times the modern value has only a moderate effect on the calculated values of $m(Ca^{2+})_i$ and $m(SO_4^{2-})_i$ (Figs. 8 and 9, Table 2).

4.2. Mesozoic and Paleozoic

Even after careful examination of many brine inclusions in the Mesozoic and Paleozoic evaporites, the composition of some of the remaining inclusions may have been modified by in-basin dolomitization. If so, this implies that $y > 0$ in Eqns. 2 and 3. Without an independent measure of the value of y, the composition of fluid inclusions can then only set minimum values on the concentration of Mg^{2+} and SO_4^{2-} and maximum values on the concentration of Ca^{2+} in seawater at the time when the inclusions were formed. As a result, the values of the $m(Mg^{2+})_i/m(Ca^{2+})_i$ ratio calculated under the assumption that dolomitization has not influenced the composition of the inclusion brines are minimum values. During periods of "calcite sea" the value of $m(Mg^{2+})_i/m(Ca^{2+})_i$ ratio in seawater at which the oceans become "aragonite sea" can be used to set an upper limit of 1.5 ± 0.5 on the $m(Mg^{2+})_i/m(Ca^{2+})_i$ ratio and hence on the effect of dolomitization on the composition of fluid inclusions formed during these periods. Similar correction can

Table 2. The composition of seawater (mmol/kg H_2O) during the Phanerozoic estimated from the composition of primary fluid inclusions in marine halite.[a]

					Fluid inclusions			$m(Mg^{2+})_i/m(Ca^{2+})_i$			Seawater		
Time	Basin	Age (Ma)	DE	N	$m(Mg^{2+})$/DE	$m(Ca^{2+})$/DE	$m(SO_4^{2-})$/DE	y = 0	limit	y-max	$m(Mg^{2+})_i$	$m(Ca^{2+})_i$	$m(SO_4^{2-})_i$
Modern seawater		0						5.2			55.1	10.6	29.2
Messinian	Red Sea	5	Br	4	43 (±7)	0	14 (±2)	3.6			43	12 (7–15)	26 (21–29)
Badenian	Eastern Europe	14	K	28	48 (±5)	0	8 (±1)	3.4			48	14 (9–18)	22 (17–26)
Oligocene	Mulhouse	35	K	2	35 (±1)	0	0	2.0			35	17 (12–21)	17 (12–21)
Eocene	Navarra	37	K	4	38 (±5)	0	3 (±1)	2.4			38	16 (11–20)	19 (14–23)
Upper Jurassic	Predobrogea	150	K	1	28	14	0	1.1 (0.9)	≤1.5	5 (8)	28–33 (36)	20–26 (19–29)	7–14 (5–19)
Upper Triassic	Lorraine	230	Br	1	28	0	1	1.6 (1.3)			≥28	≤17 (21)	≥13 (22)
Middle Triassic	Muschelkalk	240	K	1	32	0	3	2.0 (1.6)			≥32	≤16 (20)	≥14 (21)
Upper Permian	Delaware	250	Br	12	52 (±5)	0	10 (±1)	4.0 (3.1)			≥52	≤13 (17)	≥18 (19)
Lower Permian	Kansas	270	Br	1	48	0	7	3.3 (2.7)			≥48	≤14 (18)	≥16 (19)
Middle Devonian	Saskatchewan	380	Br	1	31	26	0	0.9 (0.8)	≤1.5	10 (12)	31–41 (43)	25–35 (24–38)	5–11 (3–15)
Upper Silurian	Michigan	410	Br	2	37 (±7)	21 (±3)	0	1.2 (1.1)	≤1.5	4 (7)	37–41 (44)	25–31 (25–34)	6–11 (4–15)
Late Proterozoic	Oman	550	Br	2	≥67	0	17	≥6.1 (4.7)			≥67	≤11 (14)	≥23 (17)

DE, degree of evaporation based on Br or K; N, number of analyses used in calculating DE; y, dolomite formed (mmol/kg H_2O).

[a] For the Messinian to Eocene, upper and lower limits were calculated on the basis of y = 0 (no in-basin dolomitization) and $m(Ca^{2+})_i \cdot m(SO_4^{2-})_i = 305$ (modern value) or 150–450 (in parentheses). For Triassic, Permian, and Late Proterozoic upper and lower limits were calculated on the basis of y = 0 and $m(Ca^{2+})_i \cdot m(SO_4^{2-})_i = 150$–305 or 100–450 (in parentheses). For Jurassic, Devonian and Silurian, upper and lower limits were calculated on the basis of y = 0 or $m(Mg^{2+})_i/m(Ca^{2+})_i = 1.5$ and $m(Ca^{2+})_i \cdot m(SO_4^{2-})_i = 150$–305 or 100–450 (in parentheses). $m(Mg^{2+})_i/m(Ca^{2+})_i$ is based on y = 0 and $m(Ca^{2+})_i \cdot m(SO_4^{2-})_i = 305$ or 450 (parentheses). y-max (maximum in-basin dolomitization in mmol/kg H_2O) is based on $m(Ca^{2+})_i \cdot m(SO_4^{2-})_i = 150$–305 or 100–450 (in parentheses).

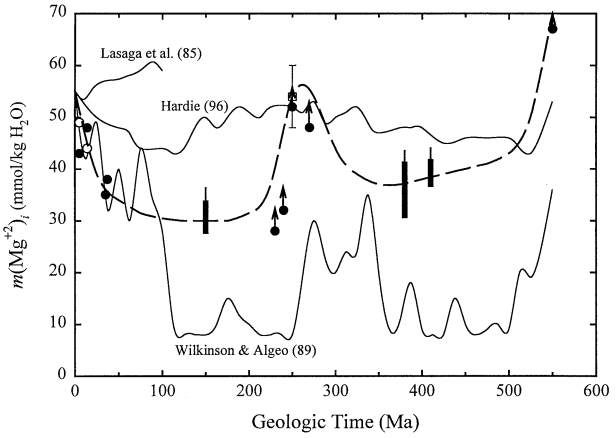

Fig. 6. Concentration of Mg^{2+} in seawater during the Phanerozoic based on analyses of fluid inclusions in marine halite (solid symbols). Thick and thin vertical bars are based on the assumption of different values for $m(Ca^{2+})_i \cdot m(SO_4^{2-})_i$. The dashed line indicates our best estimate of age curve. Open boxes = Horita et al. (1991); open circles = Zimmermann (2000a). Also shown are the results of modeling by Lasaga et al. (1985), Wilkinson and Algeo (1989), and Hardie (1996). For inclusion data, see Table 2.

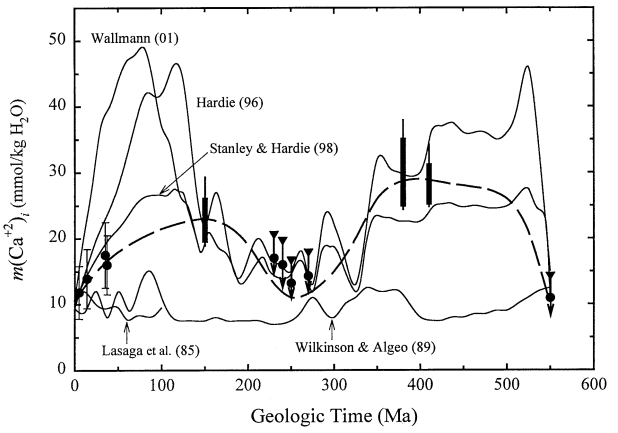

Fig. 8. Concentration of Ca^{2+} in seawater during the Phanerozoic based on analyses of fluid inclusions in marine halite (solid symbols): circles, triangles, and thick-thin vertical bars are based on the assumption of different values for $m(Ca^{2+})_i \cdot m(SO_4^{2-})_i$. The dashed line is our best estimate of the age curve. Also shown are the results of modeling by Lasaga et al. (1985), Wilkinson and Algeo (1989), Hardie (1996), Stanley and Hardie (1998), and Wallmann (2001). For inclusion data, see Table 2.

not be made for fluid inclusions that were formed during periods of "aragonite sea," because no upper limit on the $m(Mg^{2+})_i/m(Ca^{2+})_i$ ratio of seawater is set by the mineralogy of marine carbonate during these periods.

The Upper Jurassic evaporites of the Predobrogea Basin in the Ukraine formed during a period of "calcite seas," in which the upper limit of the $m(Mg^{2+})_i/m(Ca^{2+})_i$ ratio in seawater is constrained. If the products $m(Ca^{2+})_i \cdot m(SO_4^{2-})_i$ fell in the range of 150 to 305 $(mmol/kg\ H_2O)^2$, the predolomitization concentration of Mg^{2+} in seawater falls from 28 to 33 mmol/kg H_2O—that is, ~50 to 60% of the Mg^{2+} concentration of present-day seawater. The concentration of Ca^{2+} falls between 20 and 26 mmol/kg H_2O, and the concentration of SO_4^{2-} between 7 and 14 mmol/kg H_2O (Table 2). The calculated concentration of these elements changes only moderately by changing the minimum and maximum values of the product $m(Ca^{2+})_i \cdot m(SO_4^{2-})_i$ to 100 to 450 $(mmol/kg\ H_2O)^2$ (Table 2).

Triassic and Permian evaporites were deposited during a period of "aragonite seas." Thus, calculations based on the composition of inclusion brines yield only maximum values for the Ca^{2+} concentration and minimum values for the concentration of Mg^{2+} and SO_4^{2-}. The minimum concentration of Mg^{2+} in Triassic seawater ranges from 28 to 32 mmol/kg H_2O; the lower limit of the SO_4^{2-} concentration is between 13 and 14 mmol/kg H_2O (Figs. 6 and 9, Table 2). The best estimate for the maximum Ca^{2+} concentration in Triassic seawater is 16 to 17 mmol/kg H_2O (Fig. 8). In Permian seawater the concentration

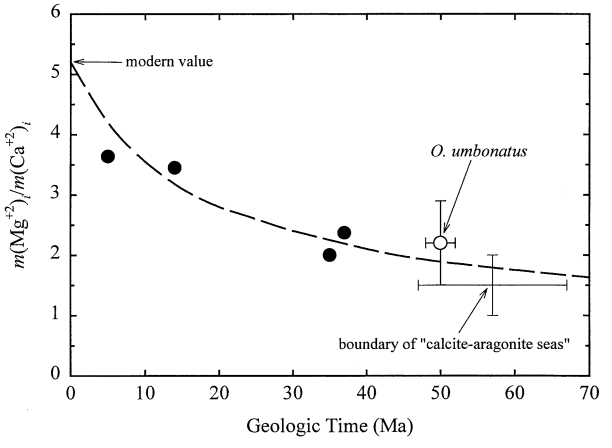

Fig. 7. $m(Mg^{2+})_i/m(Ca^{2+})_i$ ratio in seawater during the Tertiary based on analyses of fluid inclusions in marine halite (solid circles and dashed line) compared with data based on the Mg/Ca ratio of *O. umbonatus* (open circles) (Lear et al., 2000) and the boundary of the "aragonite–calcite seas" of Sandberg (1985).

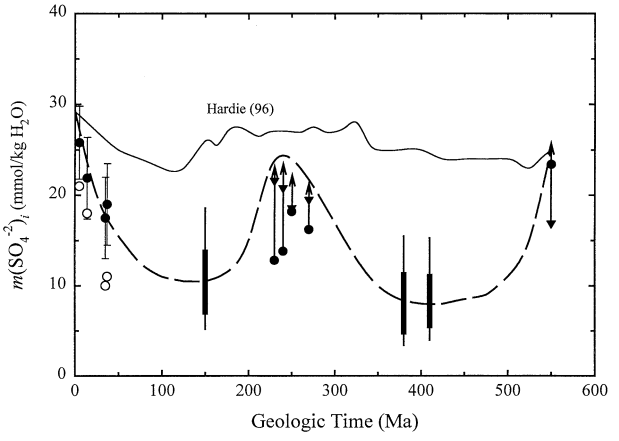

Fig. 9. Concentration of SO_4^{2-} in seawater during the Phanerozoic based on analyses of fluid inclusions in marine halite (solid symbols). Circles, triangles, and thick-thin vertical bars are based on the assumption of different values for $m(Ca^{2+})_i \cdot m(SO_4^{2-})_i$. The dashed line is our best estimate of the age curve. Open circles = Zimmermann (2000a). Also shown are the results of modeling by Hardie (1996). For inclusion data, see Table 2.

of Mg^{2+} was $\geq$48 mmol/kg H_2O, and the concentration of Ca^{2+} $\leq$14 mmol/kg H_2O. The lower limit for the SO_4^{2-} concentration in Permian seawater is 16 mmol/kg H_2O (Figs. 6, 8, and 9, Table 2). Changing the minimum and maximum values of the product $m(Ca^{2+})_i \cdot m(SO_4^{2-})_i$ to 100 to 450 (mmol/kg $H_2O)^2$ has a moderate effect on the calculated maximum and minimum concentrations of Ca^{2+} and SO_4^{2-}, respectively (Table 2, Figs. 8 and 9).

Inclusion fluids in Devonian and Silurian marine evaporites, which formed during a period of "calcite seas," may also have been affected by in-basin dolomitization. Our calculations result in a range of Mg^{2+} concentrations in seawater of 31 to 41 mmol/kg H_2O for the Devonian and 37 to 41 mmol/kg H_2O for the Silurian. The concentration of Ca^{2+} in Devonian and Silurian seawater ranges from 25 to 35 mmol/kg H_2O, the SO_4^{2-} concentration from 5 to 11 mmol/kg H_2O (Table 2). The use of 100 and 450 (mmol/kg $H_2O)^2$ for the minimum and maximum values of the product $m(Ca^{2+})_i \cdot m(SO_4^{2-})_i$, increases the range of the calculated concentration of these elements somewhat.

4.3. Late Proterozoic

The Late Proterozoic Ara Formation in Oman can also be used to constrain the composition of seawater. Most of the inclusion brines analyzed appear to be saturated with respect to potash minerals and $MgSO_4$ minerals as discussed before. Thus, only lower limits are constrained: $m(K^+)_i \geq 9$ mmol/kg H_2O; $m(Mg^{2+})_i \geq 67$ mmol/kg H_2O; $m(SO_4^{2-})_i \geq 17$ to 23 mmol/kg H_2O; $m(Ca^{2+})_i \leq 11$ to 14 mmol/kg H_2O (Table 2, Figs. 6, 8, and 9).

4.4. Secular Changes during the Phanerozoic

On the basis of the reconstructed composition of seawater during the Tertiary, Jurassic, Triassic, Permian, Devonian, Silurian, and Late Proterozoic, our best estimates of the evolution of the concentration of K^+, Mg^{2+}, Ca^{2+} and SO_4^{2-} in Phanerozoic seawater are shown in Figures 5 to 9. Although the composition of seawater is well documented for only a few geologic periods, the major features of secular changes in the composition of seawater have emerged. Our results clearly demonstrate that the composition of seawater has changed significantly during the past 600 myr. The variation of the Mg^{2+} concentration in Phanerozoic seawater mimics the stand of sea level (Vail et al., 1977). At low stands of sea level at the present and during the Permian and the Late Neoproterozoic, the concentration of Mg^{2+} in seawater was $\geq$50 mmol/kg H_2O. During high stands of sea level in the Cretaceous/Jurassic and Devonian to Early Cambrian the concentration of Mg^{2+} in seawater was significantly lower, in the range of 30 to 40 mmol/kg H_2O. The SO_4^{2-} concentration varied from values as low as 5 to 10 mmol/kg H_2O to near-present values of 28 mmol/kg H_2O in phase with Mg^{2+} (Fig. 9). On the other hand, the Ca^{2+} concentration in seawater was high during the Cretaceous/Jurassic and the Devonian to Early Cambrian, and similar to its present value during the Late Neoproterozoic and the Permian (Fig. 8). The trends of Mg^{2+} and SO_4^{2-} appear to be mirror images of Ca^{2+}. Because of this inverse relationship between the estimated Ca^{2+} and Mg^{2+} concentrations in seawater, the $m(Mg^{2+})_i/m(Ca^{2+})_i$ ratio has changed by a factor of

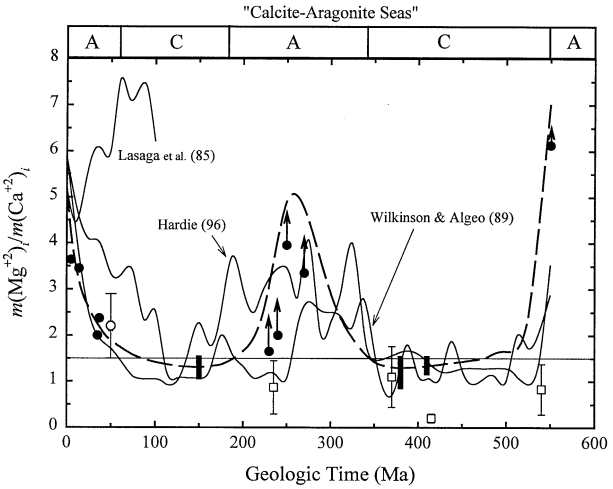

Fig. 10. $m(Mg^{2+})_i/m(Ca^{2+})_i$ ratio in seawater during the Phanerozoic based on analyses of fluid inclusions in marine halite (solid symbols and dashed line) compared with the data based on Mg/Ca of *O. umbonatus* (open circles) (Lear et al., 2000) and of abiogenic marine carbonate cements (open squares) (after Cicero and Lohmann, 2001). Also shown are the results of modeling by Lasaga et al. (1985), Wilkinson and Algeo (1989), and Hardie (1996). "A" and "C" at the top indicate the aragonite and calcite seas of Sandberg (1985). For inclusion data, see Table 2.

~5 in phase with the alternating "calcite-seas" and "aragonite-seas" of Sandberg (1983, 1985) (Fig. 10). Lowenstein et al. (2001) reached similar conclusion regarding the secular variations in the $m(Mg^{2+})_i/m(Ca^{2+})_i$ ratio during the Phanerozoic. This is not surprising because many of their halite samples were obtained from the same evaporite deposits as ours and because they used the same literature data.

Siemann (2000) showed that the Br content of basal halite from many Phanerozoic marine evaporite deposits ranges between 30 and 100 ppm. He argued that these changes can be readily explained by major changes in the chemistry of seawater similar to those proposed by Hardie (1996).

Cicero and Lohmann (2001) have compiled trace element (Mg and Sr) concentration data for Holocene, Pliocene, M. Triassic, Late Devonian, Late Silurian, and Early Cambrian abiogenic marine carbonate cements, and have suggested that the concentration of these elements can be used to estimate their concentration in seawater. If the Mg concentration of these marine calcite cements was determined solely by the $m(Mg^{2+})_i/m(Ca^{2+})_i$ ratio in contemporaneous seawater, this ratio in Middle Triassic, Late Devonian, Late Silurian, and Early Cambrian seawater could be evaluated (Fig. 10). Low $m(Mg^{2+})_i/m(Ca^{2+})_i$ ratios obtained in this way, particularly those for Late Silurian seawater, probably reflect the complexity of the processes that govern the distribution of trace elements in marine carbonate cements and possibly the effects of diagenesis.

5. CAUSES OF THE SECULAR CHANGES IN THE COMPOSITION OF SEAWATER

During the past two decades, a number of models have been proposed for the chemical evolution of seawater during the Phanerozoic. Several of these are compared with ours in Fig-

ures 5 to 10. The Berner-Lasaga-Garrels (BLAG) box model developed by Berner et al. (1983) and Lasaga et al. (1985) included all of the major geochemical processes that affect the composition of seawater. Their changes in the concentration of Mg^{2+} and Ca^{2+} during the past 100 myr are, however, much smaller than our estimates (Figs. 6 and 8). The differences are due in part to the absence of dolomite as a major sink of Mg^{2+} in the BLAG model. On the other hand, Wallmann (2001) proposed concentrations of Ca^{2+} much higher than our estimates (Fig. 8) because he assumed, as an initial value in his model, that at 150 Ma the Ca^{2+} concentration in seawater was twice that of modern seawater.

The effect of penecontemporaneous dolomite deposition on the chemical evolution of seawater was included in the model published by Wilkinson and Algeo (1989), which was based on Given and Wilkinson's (1987) compilation of the distribution of limestones and dolomites in Phanerozoic sediments. Their calculations suggest that the concentration of Ca^{2+} in seawater remained relatively constant ($\pm$20%) during the Phanerozoic, but that the concentration of Mg^{2+} changed significantly, largely in phase with their proposed dolomite-age curve (Figs. 6 and 8). The changes that they proposed for the concentration of both elements differ significantly from those in our model, in part because of their incomplete compilation of Phanerozoic carbonate rocks (Holland and Zimmermann, 2000).

A decided step forward was taken by Spencer and Hardie (1990) and Hardie (1996), who based their model on changes in the mixing ratio of river water and hydrothermal fluids generated by MORs. Hardie (1996) assumed that the flux of MOR hydrothermal fluids has varied linearly with the rate of seafloor spreading. For the past 150 myr this rate can be estimated directly from the distribution of seafloor ages. For times before 150 Ma Hardie (1996) used the first-order global sea-level curve (Gaffin, 1987) and the abundance of granitic plutons (Engel and Engel, 1964) as a proxy for the spreading rate of MORs. Hardie's (1996) calculations suggest that the concentration of Ca^{2+} and K^{+} in seawater has undergone 4-5 fold secular changes in phase with crustal production rates during the past 540 myr. The concentration of these elements in modern seawater represents minima for both elements. The concentration of other elements (Mg^{2+}, SO_4^{2-}, etc.) is proposed to have changed only moderately. Hardie's (1996) calculations suggest that seawater was of the Ca-Cl type during the early and middle Phanerozoic, the Cretaceous, and the early and middle Cenozoic. These predictions are consistent with the mineralogy of marine potash deposits ($MgSO_4$ vs. KCl potash deposits) and the mineralogy of marine skeletal limestones ("aragonite-calcite seas"). Stanley and Hardie (1998) have expanded the Hardie hypothesis, arguing that secular changes in the $m(Mg^{2+})_i/m(Ca^{2+})_i$ ratio of seawater driven by changes in the flux of MOR fluids has also controlled the mineralogy of hypercalcifying algae.

Hardie's calculations (Hardie, 1996; Stanley and Hardie, 1998) agree reasonably well with our age-curve for $m(Ca^{2+})_i$ and for the $m(Mg^{2+})_i/m(Ca^{2+})_i$ ratio (Figs. 8 and 10). They differ significantly from our age curves for $m(Mg^{2+})_i$ and $m(SO_4^{2-})_i$ (Figs. 6 and 9). The differences between our age-curves and those of Hardie (1996) are due in part to the simplicity of his model. The chemical evolution of seawater is clearly controlled by many factors other than the mixing of present-day river waters with present-day hydrothermal fluids (Holland et al., 1996). However, some of the differences are probably due also to the inadequacy of the available fluid inclusion data and the uncertainties in their interpretation. A more definitive model for the chemical evolution of seawater will emerge when analyses of inclusion fluids consisting of unevaporated seawater become available.

What is already clear is that the composition of seawater has responded to tectonic forcing and to biologic evolution. Fischer (1984) was the first to recognize two supercycles in the Earth's exogenic processes during the Phanerozoic. These cycles included eustatic changes of sea level, changes in climate, and biotic crises. He related these cycles to mantle convection, plate motions, and continental drift and showed how these processes can serve to explain many of the long-term changes in the sedimentary record as well as the two supercycles in the composition of seawater.

Global tectonics do not, however, explain the significant changes in the composition of seawater during the past 40 myr because the rate of seafloor spreading seems to have been nearly constant during most of the Tertiary (Lithgow-Bertelloni et al., 1993). Holland and Zimmermann (2000) have proposed that the changes in the Mg^{2+}, Ca^{2+}, and SO_4^{2-} concentration of seawater during this period are due to the decrease in the global rate of dolomite formation. This decrease was occasioned by the gradual transfer of $CaCO_3$ deposition from shallow- to deep-water settings due to the proliferation of marine planktonic calcareous organisms. If this explanation is correct, the composition of seawater has been influenced by biologic evolution as well as by tectonic processes. At present we seem to have a reasonable qualitative explanation for the chemical evolution of seawater during the Phanerozoic. A quantitative model is still lacking. Its development is surely one of the most intriguing challenges of paleoceanography.

Acknowledgments—We acknowledge stimulating discussions with L. A. Hardie, T. K. Lowenstein and his group at SUNY Binghamton, and A. B. Carpenter. The late Bill Holser shared his extensive knowledge of marine evaporites with us. Lynn Walter and Jeff Hanor provided many helpful suggestions for improving the manuscript. The halite samples investigated in this study were kindly provided by many people (A. B. Carpenter, W. T. Holser, V. M. Kovalevich, L. S. Land, M. Moge, O. I. Petrichenko, G. E. Williams, and I. Zak), the Deep Sea Drilling Project (currently the Ocean Drilling Project), and Petroleum Development Oman. Funding for this project was provided by NSF, NASA (NAG5-4174), the Deutsche Forschungsgemeinschaft (Zi 418/1), and the Division of Chemical Sciences, Geosciences, and Biosciences, Office of Basic Energy Sciences, U.S. Department of Energy, under contract DE-AC05-00OR22725, Oak Ridge National Laboratory, managed and operated by UT-Battelle, LLC.

Associate editor: L. M. Walter

REFERENCES

Ayora C. and Fontarnau R. (1990) X-ray microanalysis of frozen fluid inclusions. *Chem. Geol.* **89,** 135–148.

Ayora C., Garçia-Veigas J., and Pueyo J.-J. (1994a) X-ray microanalysis of fluid inclusions and its application to the geochemical modelling of evaporite basins. *Geochim. Cosmochim. Acta* **58,** 43–55.

Ayora C., Garçia-Veigas J., and Pueyo J.-J. (1994b) The chemical and hydrological evolution of an ancient potash-forming evaporite basin as constrained by mineral sequence, fluid inclusion composition, and numerical simulation. *Geochim. Cosmochim. Acta* **58,** 3379–3394.

Ayora C., Cendón D. I., Taberner C., and Pueyo J. J. (2001) Brine–

mineral reactions in evaporite basins: Implications for the composition of ancient oceans. *Geology* **29,** 251–254.

Banerjee D. M., Strauss H., Bhattacharya S. K., Kumar V., and Mazumdar A. (1998) Isotopic composition of carbonates and sulphates, potash mineralisation and basin architecture of the Nagaur-Ganganagar evaporite basin (north-western India) and their implications on the Neoproterozoic exogene cycle. *Mineral. Mag.* **62A,** 106–107.

Banerjee D. M. and Mazumdar A. (1999) On the Late Neoproterozoic–early Cambrian transition events in parts of East Gondwanaland. *Gondwana Res.* **2,** 199–211.

Bein A., Hovorka S. D., Fisher R. S., and Roedder E. (1991) Fluid inclusions in bedded Permian halite, Palo Duro Basin, Texas: Evidence for modification of seawater in evaporite brine-pools and subsequent early diagenesis. *J. Sediment. Petrol.* **61,** 1–14.

Belmonte Y., Hirtz P., and Wenger R. (1965) The salt basins of the Gabon and the Congo (Brazzaville)—A tentative palaeogeographic interpretation. In *Salt Basins around Africa*, pp. 55–74. Institute of Petroleum.

Berner R. A., Lasaga A. C., and Garrels R. M. (1983) The carbonate–silicate geochemical cycle and its effect on atmospheric carbon dioxide over the past 100 million years. *Am. J. Sci.* **283,** 641–683.

Borchert H. and Muir R. O. (1964) *Salt Deposits: The Origin, Metamorphism and Deformation of Evaporites.* Van Nostrand.

Braitsch O. (1971) *Salt Deposits: Their Origin and Composition.* Springer-Verlag.

Broecker W. S. (1971) A kinetic model for the chemical composition of sea water. *Quat. Res.* **1,** 188–207.

Bukowski K., Galamay A. R., and Góralski M. (2000) Inclusion brine chemistry of the Badenian salt from Wieliczka. *J. Geochem. Explor.* **69/70,** 87–90.

Canals A., Carpentier B., Huc A. Y., Guilhaumou N., and Ramsey M. H. (1993) Microanalysis of primary fluid inclusions in halite; constraints for an evaporitic sedimentation modeling: Application to the Mulhouse Basin (France). *Org. Geochem.* **20,** 1139–1151.

Cathro D. L., Warren J. K., and Williams G. E. (1992) Halite saltern in the Canning Basin, Western Australia: A sedimentological analysis of drill core from the Ordovician–Silurian Mallowa Salt. *Sedimentology* **39,** 983–1002.

Cicero A. D. and Lohmann K. C. (2001) Sr/Mg variation during rock–water interaction: Implications for secular changes in the elemental chemistry of ancient seawater. *Geochim. Cosmochim. Acta* **65,** 741–761.

Clement G. P. and Holser W. T. (1988) Geochemistry of Moroccan evaporites in the setting of the North Atlantic Rift. *J. Afr. Earth Sci.* **7,** 375–383.

Das N., Horita J., and Holland H. D. (1990) Chemistry of fluid inclusions in halite from the Salina Group of the Michigan Basin: Implications for Late Silurian seawater and the origin of sedimentary brines. *Geochim. Cosmochim. Acta* **54,** 319–327.

Das Gupta S. P., Kumar V., Ramchandra, and Jairam M. S. (1988) A framework of the Nagaur-Ganganagar evaporite basin, Rajasthan. *Indian Minerals* **42,** 57–64.

El Tabakh M., Utha-Aroon C., and Schreiber B. C. (1999) Sedimentology of the Cretaceous Maha Sarakham evaporites in the Khorat Plateau of northeastern Thailand. *Sediment. Geol.* **123,** 31–62.

Engel A. E. J. and Engel C. G. (1964) Continental accretion and the evolution of North America. In *Advancing Frontiers in Geology and Geophysics* (eds. A. P. Subramaniam and A. P. Balakrishna), pp. 17–37. Indian Geophysical Union.

Eugster H. P., Harvie C. E., and Weare J. H. (1980) Mineral equilibria in a six-component seawater system, Na-K-Mg-Ca-SO_4-Cl-H_2O, at 25°C. *Geochim. Cosmochim. Acta* **44,** 1335–1347.

Fanlo I. and Ayora C. (1998) The evolution of the Lorraine evaporite basin: Implications for the chemical and isotope composition of the Triassic ocean. *Chem. Geol.* **146,** 135–154.

Fischer A. G. (1984) The two Phanerozoic supercycles. In *Catastrophes and Earth History* (eds. W. A. Berggren and J. A. Van Couvering), pp. 129–150. Princeton University Press.

Folle S. and Beutel T. (2000) Overview of salt occurrence in the Persian Gulf and Red Sea Region. In *Proceedings of the 8th World Salt Symposium*, Vol. 1. (ed. R. Geertmann), pp. 119–124. Elsevier.

Füchtbauer H. and Hardie L. A. (1976) Experimentally determined homogeneous distribution coefficients for precipitated magnesian calcites: Application to marine carbonate cement [abstract]. In *Program and Abstracts of the Geological Society of America*, Vol. 8, p. 877. Geological Society of America.

Gaffin S. (1987) Ridge volume dependence on seafloor generation rate and inversion using long term sealevel change. *Am. J. Sci.* **287,** 596–611.

Galamay A. R. and Karoli S. (1997) Geochemistry of the Badenian salts from the East Slovakian Basin, Slovakia. *Slovak Geol. Mag.* **3,** 187–192.

Galamay A. R., Bukowski K., and Przybylo J. (1997) Chemical composition and origin of brines in the Badenian evaporite basin of the Carpathian Foredeep: Fluid inclusion data from Wieliczka (Poland). *Slovak Geol. Mag.* **3,** 165–171.

Garçia-Veigas J., Orti F., Rosell L., Ayora C., Rouchy J.-M., and Lugli S. (1995) The Messinian salt of the Mediterranean: Geochemical study of the salt from the Central Sicily Basin and comparison with the Lorca Basin (Spain). *Bull. Soc. Geol. France* **166,** 699–710.

Garçia-Veigas J., Rossel L., and Garlicki A. (1997) Petrology and geochemistry (fluid inclusions) of Miocene halite rock salts (Badenian, Poland). *Slovak Geol. Mag.* **3,** 181–186.

Garrett D. E. (1996) *Potash-Deposits, Processing, Properties and Uses.*Chapman and Hall.

Given R. K. and Wilkinson B. H. (1987) Dolomite abundance and stratigraphic age: Constraints on rates and mechanisms of Phanerozoic dolostone formation. *J. Sediment. Petrol.* **57,** 1068–1078.

Gorin G. E., Racz L. G., and Walter M. R. (1982) Late Precambrian–Cambrian sediments of Huqf Group, Sultanate of Oman. *AAPG Bull.* **66,** 2609–2627.

Grishina S., Dubessy J., Kontorovich A., and Pironon J. (1992) Inclusions in salt beds resulting from thermal metamorphism by dolerite sills (eastern Siberia, Russia). *Eur. J. Mineral.* **4,** 1187–1202.

Hardie L. A. (1990) The roles of rifting and hydrothermal $CaCl_2$ brines in the origin of potash evaporites: An hypothesis. *Am. J. Sci.* **290,** 43–106.

Hardie L. A. (1996) Secular variation in seawater chemistry: An explanation for the coupled variation in the mineralogies of marine limestones and potash evaporites over the past 600 my. *Geology* **24,** 279–283.

Harvie C. E., Møller N., and Weare J. H. (1984) The prediction of mineral solubilities in natural waters: The Na-K-Mg-Ca-H-Cl-SO_4-OH-HCO_3-CO_3-CO_2-H_2O system to high ionic strengths at 25°C. *Geochim. Cosmochim. Acta* **48,** 723–751.

Herrmann A. G. (1991) Fraktionierung im Stoffbestand der Zechsteinevaporite Mittel- und Norddeutschlands. *Zbl. Geol. Paläont.* **1,**1091–1106.

Herrmann A. G., Rühe S., and Usdowski E. (1997) Fluid Inclusions: Neue Erkenntnisse über den Stoffbestand NaCl-gesättigter Meerwasserlösungen im Zechstein 3. *Kali Steinsalz* **12,** 115–124.

Hite R. J. (1985) The sulfate problem in marine evaporites. In *6th International Symposium on Salt* (eds. B. C. Schreiber and H. L. Harner), pp. 217–230. Salt Institute.

Hite R. J. and Japakasetr T. (1979) Potash deposits of the Khorat Plateau, Thailand and Laos. *Econ. Geol.* **74,** 448–458.

Holland H. D. (1972) The geologic history of sea water—An attempt to solve the problem. *Geochim. Cosmochim. Acta* **36,** 637–651.

Holland H. D. (1978) *The Chemistry of the Atmosphere and the Oceans.*Wiley.

Holland H. D. (1984) *The Chemical Evolution of the Atmosphere and Oceans.*Princeton University Press.

Holland H. D., Horita J., and Seyfried W. E. (1996) On the secular variations in the composition of Phanerozoic marine potash evaporites. *Geology* **24,** 993–996.

Holland H. D. and Zimmermann H. (1998) On the secular variations in the composition of Phanerozoic marine potash evaporites: Comment and reply. *Geology* **26,** 91–92.

Holland H. D. and Zimmermann H. (2000) The dolomite problem revisited. *Int. Geol. Rev.* **42,** 481–490.

Holser W. T. (1963) Chemistry of brine inclusion in Permian salt from Hutchinson, Kansas. In *1st Symposium on Salt*(ed. A. C. Bersticker), pp. 86–95. Northern Ohio Geological Society.

Holser W. T. and Wilgus C. K. (1981) Bromide profiles of the Röt Salt,

Triassic of northern Europe, as evidence of its marine origin. *N. Jb. Miner. Mh.* **6,** 267–276.

Horita J., Friedman T. J., Lazar B., and Holland H. D. (1991) The composition of Permian seawater. *Geochim. Cosmochim. Acta* **55,** 417–432.

Horita J., Weinberg A., Das N., and Holland H. D. (1996) Brine inclusions in halite and the origin of the Middle Devonian Prairie Evaporites of Western Canada. *J. Sediment. Res.* **66,** 956–964.

Jones C. L. (1970) Potash in halitic evaporites, Salt Range, West Pakistan. Professional Paper 700D. U.S. Geological Survey.

Khmelevska E. V. (1997) Upper Jurassic evaporites of the southwestern slope of East European Platform. *Slovak Geol. Mag.* **3,** 213–216.

Kovalevich V. M. and Petrichenko O. I. (1997) Chemical composition of brines in Miocene evaporite basins of the Carpathian region. *Slovak Geol. Mag.* **3,** 173–180.

Kovalevich V. M., Jarmolowicz-Szulc K., Peryt T. M., and Poberegski A. V. (1997) Messinian chevron halite from the Red Sea (DSDP sites 225 and 227): Fluid inclusion study. *Neues Jb. Miner. Mh.* **10,** 433–450.

Kovalevich V. M., Peryt T. M., and Petrichenko O. I. (1998) Secular variation in seawater chemistry during the Phanerozoic as indicated by brine inclusions in halite. *J. Geol.* **106,** 695–712.

Kovalevich V. M. and Hauber L. (2000) Fluid inclusions in halite from the Middle Triassic salt deposits in northern Switzerland: Evidence for seawater chemistry. In *Proceedings of the 8th World Salt Symposium*, Vol. 1. (ed. R. Geertmann), pp. 143–148. Elsevier.

Land L. S., Eustice R. A., Mack L. E., and Horita J. (1995) Reactivity of evaporites during burial: An example from the Jurassic of Alabama. *Geochim. Cosmochim. Acta* **59,** 3765–3778.

Lasaga A. C., Berner R. A., and Garrels R. M. (1985) An improved geochemical model of atmospheric CO_2 fluctuations over the past 100 million years. In *The Carbon Cycle and Atmospheric CO_2, Natural Variations Archean to Present* (ed. E. T. Sundquist and W. S. Broecker), pp. 397–411. Geophysics Monograph 32. American Geophysics Union.

Lazar B. and Holland H. D. (1988) The analysis of fluid inclusions in halite. *Geochim. Cosmochim. Acta* **52,** 485–490.

Lear C. H., Elderfield H., and Wilson P. A. (2000) Cenozoic deep-sea temperatures and global ice volumes from Mg/Ca in benthic foraminiferal calcite. *Science* **287,** 269–272.

Lithgow-Bertelloni C., Richards M. A., and Ricard Y., O'Connell R. J., and Engebretson D. C. (1993) Toroidal-poloidal partitioning of plate motions since 120 Ma. *Geophys. Res. Lett.* **20,** 375–378.

Lowenstein T. K., Timofeeff M. N., Hardie L. A. and Brennan S. T. (1999) Evaluating secular changes in seawater chemistry. In *Program and Abstracts of the 9th Annual V. M. Goldschmidt Conference*, Lunar and Planetary Institute, pp. 176–177.

Lowenstein T. K. Timofeeff M. N., Brennan S. T., Hardie L. A. and Demicco R. V. (2001) Oscillations in Phanerozoic seawater chemistry: Evidence from fluid inclusions in salt deposits. *Science* **294,** 1086–1088.

McCaffrey M. A., Lazar B., and Holland H. D. (1987) The evaporation path of seawater and the coprecipitation of Br^- and K^+ with halite. *J. Sediment. Petrol.* **57,** 928–937.

Mackenzie F. T. and Garrels R. M. (1966) Chemical mass balance between rivers and oceans. *Am. J. Sci.* **264,** 507–525.

Mattes B. W. and Morris S. C. (1990) Carbonate/evaporite deposition in the Late Precambrian–Early Cambrian Ara-Formation of Southern Oman. In *The Geology and Tectonics of the Oman Region* (eds. A. H. F. Robertson, M. P. Searle, and A. C. Ries), pp. 617–636. Special Publication 49. Geological Society.

Maynard J. B. (1976) The long-term buffering of the oceans. *Geochim. Cosmochim. Acta* **40,** 1523–1532.

Menning M. (1995) A numerical time scale for the Permian and Triassic Periods: An integrated time analysis. In *The Permian of Northern Pangea*, Vol. 1, *Paleogeography, Paleoclimates, Stratigraphy* (eds. P. A. Scholle, T. M. Peryt, and D. S. Ulmer-Scholle), pp. 77–97. Springer.

Morse J. W., Wang Q., and Tsio M.-Y. (1997) Influences of temperature and Mg:Ca ratio on $CaCO_3$ precipitates from seawater. *Geology* **25,** 85–87.

Peryt T. M. and Kovalevich V. M. (1996) Origin of anhydrite pseudomorphs after gypsum crystals in the Oldest Halite (Werra, Upper Permian, northern Poland). *Zbl. Geol. Paläont.* **1, 337–356.**

Peters H. (1988) Stoffbestand und Genese des Kaliflözes Riedel (K3Ri) im Salzstock Wathlingen-Hänigsen, Werk Niedersachsen-Riedel. Dissertation, Universität Göttingen.

Petrichenko O. I. (1973) Methods of study of inclusions in minerals of saline deposits, Naukova Dumka, Kiev. In Ukrainian; translated in *Fluid Inclusions Res.* **12,** 214–274, 1979.

Petrychenko O. I., Peryt T. M., and Roulston B. (in press) Seawater composition during deposition of Viséan evaporites in the Moncton Subbasin of New Brunswick as inferred from the fluid inclusion study of halite. *Can. J. Earth Sci.*

Rubey W. W. (1951) The geologic history of sea water—An attempt to state the problem. *Geol. Soc. Am. Bull.* **62,** 1111–1147.

Sandberg P. A. (1983) An oscillating trend in Phanerozoic non-skeletal carbonate mineralogy. *Nature* **305,** 19–22.

Sandberg P. A. (1985) Nonskeletal aragonite and pCO_2 in the Phanerozoic and Proterozoic. In *The Carbon Cycle and Atmospheric CO_2, Natural Variations Archean to Present* (ed. E. T. Sundquist and W. S. Broecker), pp. 585–594. Geophysics Monograph 32. American Geophysics Union.

Shaidetska V. S. (1997) Geochemistry of Neogene evaporites of the Transcarpathian Trough in Ukraine. *Slovak Geol. Mag.* **3,** 193–200.

Shepherd T. J. and Chenery S. R. (1995) Laser ablation ICP-MS elemental analysis of individual fluid inclusions: An evaluation study. *Geochim. Cosmochim. Acta* **59,** 3997–4007.

Shepherd T. J., Ayora C., Cendón D. I., Chenery S. R., and Moissette A. (1998) Quantitative solute analysis of single fluid inclusions in halite by LA-ICP-MS and cryo-SEM-EDS: Complementary microbeam techniques. *Eur. J. Mineral.* **10,** 1097–1108.

Siemann M. G. (2000) Response of chemical sediments on possible changes in Phanerozoic seawater composition. In *Program and Abstracts of the Geological Society of America*, Vol. 32. Geological Society of America, p. A67.

Sillén L. G. (1961) The physical chemistry of sea water. In *Oceanography* (ed. M. Sears), pp. 549–581. Publication 67. American Association for the Advancement of Science.

Sillén L. G. (1967) The ocean as a chemical system. *Science* **156,** 1189–1197.

Spencer R. J. and Hardie L. A. (1990) Control of seawater composition by mixing of river waters and mid-ocean ridge hydrothermal brines. In *Fluid–Mineral Interactions: A Tribute to H. P. Eugster* (eds. R. J. Spencer and I.-M. Chou), pp. 409–419. Special Publication 2. Geochemical Society.

Stanley S. M. and Hardie L. A. (1998) Secular oscillations in the carbonate mineralogy of reef-building and sediment-producing organisms driven by tectonically forced shifts in seawater chemistry. *Paleogeogr. Paleoclimatol. Paleoecol.* **144,** 3–19.

Stein C. L. and Krumhansl J. L. (1988) A model for the evolution of brines in salt from the lower Salado Formation, southeastern New Mexico. *Geochim. Cosmochim. Acta* **52,** 1037–1046.

Stein M., Starinsky A., Agnon A., Katz A., Raab M., Spiro B., and Zak I. (2000) The impact of brine–rock interaction during marine evaporite formation on the isotopic Sr record in the oceans: Evidence from Mt. Sedom, Israel. *Geochim. Cosmochim. Acta* **64,** 2039–2053.

Tew B. H., Mink R. M., Mann S. D., Bearden B. L., and Mancini E. A. (1991) Geologic framework of Norphlet and pre-Norphlet strata of the onshore and offshore eastern Gulf of Mexico area. *Trans. Gulf Coast Assn. Geol. Soc.* **41,** 590–600.

Timofeeff M. N., Lowenstein T. K., and Hardie L. A. (1999) Chemical composition of Cretaceous seawater: Results from environmental scanning electron microscope–energy dispersive X-ray spectrometry analyses of fluid inclusions in marine halites. In *Program and Abstracts of the 9th Annual V. M. Goldschmidt Conference*, Lunar and Planetary Institute, p. 299.

Timofeeff M. N., Lowenstein T. K., and Blackburn W. H. (2000) ESEM-EDS: An improved technique for major element chemical analysis of fluid inclusions. *Chem. Geol.* **164,** 171–182.

Timofeeff M. N., Lowenstein T. K., Brennan S. T., Demicco R. V., Zimmermann H., Horita J., and von Borstel L. E. (2001) Evaluating seawater chemistry from fluid inclusions in halite: Examples from

modern marine and nonmarine environments. *Geochim. Cosmochim. Acta* **65,** 2293–2300.

Usdowski E. and Dietzel M. (1998) *Atlas and Data of Solid-Solution Equilibria of Marine Evaporites.* Springer-Verlag.

Vail P. R., Mitchum R. M. Jr., and Thompson S. III. (1977) Global cycles of relative changes of sea level. In *Seismic Stratigraphy and Global Changes of Sea Level* (ed. C. E. Payton), pp. 83–97. Memoir 26. Am. Assoc. Petrol. Geol.

von Borstel L. E., Zimmermann H., and Ruppert H. (2000) Fluid inclusion studies in modern halite from the Inagua solar saltwork. In *Proceedings of the 8th World Salt Symposium*, Vol. 1. (ed. R. Geertmann), pp. 673–678. Elsevier.

Wallmann K. (2001) Controls on the Cretaceous and Cenozoic evolution of seawater composition, atmospheric CO_2 and climate. *Geochim. Cosmochim. Acta* **65,** 3005–3025.

Wardlaw N. C. (1972) Unusual marine evaporites with salts of calcium and magnesium chloride in Cretaceous basins of Sergipe, Brazil. *Econ. Geol.* **67,** 156–168.

Wilkinson B. H. and Algeo T. J. (1989) Sedimentary carbonate record of calcium–magnesium cycling. *Am. J. Sci.* **289,** 1158–1194.

Zak I. (1997) Evolution of the Dead Sea brines. In *The Dead Sea: The Lake and Its Setting*(eds. T. M. Niemi, Z. Ben-Avraham, and J. R. Gat), pp. 133–144. Oxford University Press.

Zimmermann H. (2000a) Tertiary seawater chemistry—Implications from fluid inclusions in primary marine halite. *Am. J. Sci.* **300,** 723–767.

Zimmermann H. (2000b) *The Evolution of Seawater during the Past 40 Ma: Evidence from the Mineralogy of Marine Evaporites and Fluid Inclusions in Marine Halite.* Habilitationsschrift, Universität Göttingen.

Zimmermann H. (2001) On the origin of fluids included in Phanerozoic marine halite—Basic interpretation strategies. *Geochim. Cosmochim. Acta* **65,** 35–45.

Appendix. Composition of major species and Jänecke units of fluid inclusions in Phanerozoic marine halite from this study and from the literature.[a]

	Stratigraphy/basin		Sample	Inclusion type	Method	Na	K	Mg	Ca	Cl	SO_4	Br	Li	CB	Mg	2K	SO_4	Ca
						(mmol/kg H_2O)								(%)	Jänecke unit (%)			
					Plio-Pleistocene: Sedom Formation, Israel (this study)													
	Dead Sea	Sedom	IZ2-1	ch	Extraction-IC	1240	377	3110		7170	70	61.2		2.7	85.3	12.3	2.4	
	Dead Sea	Sedom	IZ2-2	ch	Extraction-IC	939	551	3190		7680	130	56.6		1.1	90.4	8.8	0.9	
	Dead Sea	Sedom	IZ2-3	ch	Extraction-IC	1240	868	2840		7710	78	62.5		2.9	83.3	10.4	6.3	
	Dead Sea	Sedom	IZ3-1	ch	Extraction-IC	740	757	3470		8460	33	73.8		2.9	86.6	8.3	5.1	
	Dead Sea	Sedom	IZ3-2	ch	Extraction-IC	1530	760	2640		7220	76	59.5		2.8	82.0	10.0	8.0	
	Dead Sea	Sedom	IZ3-3	ch	Extraction-IC	810	665	3430		8180	33	70.1		1.3	83.6	10.0	6.4	
sw	Dead Sea	Sedom	IZ5(1)-1	ch	Extraction-IC	1860	609	2440		6770	185	47.9		1.2	89.6	6.2	4.1	
	Dead Sea	Sedom	IZ5(1)-2	ch	Extraction-IC	1200	584	3030		7260	178	46.1		−1.7	86.1	11.3	2.5	
	Dead Sea	Sedom	IZ5(2)-1	ch	Extraction-IC	2050	569	2330		6620	228	38.1		−0.5	83.4	12.3	4.3	
					Extraction-IC													
					Miocene, Messinian: Red Sea (Lazar and Holland, personal communication)													
sw*	DSDP-227		30-2/2	ch	Extraction-IC	3520	362	1550		6170	479	29.1		−2.1	70.1	8.2	21.7	
sw*	DSDP-227		32-4/2	ch	Extraction-IC	2910	618	1960		6050	598	52.3		2.7	68.4	10.8	20.9	
sw*	DSDP-227		35-5/1	ch	Extraction-IC	3500	370	1600		6170	490	30.8		−1.1	70.3	8.1	21.5	
sw*	DSDP-227		35-5/3	ch	Extraction-IC	3630	371	1580		6400	536	29.2		−4.3	68.7	8.1	23.3	
					Miocene, Messinian: Red Sea (Kovalevich et al., 1997)													
sw	DSDP-227		35-1/110-112	ch	Petrichenko		178	1104			299				74.0	6.0	20.0	
sw	DSDP-227		43-4/015-017	ch	Petrichenko		206	1158			361				71.4	6.4	22.2	
sw	DSDP-225		27-2/110-112	ch	Petrichenko		249	1145			231				76.3	8.3	15.4	
sw	DSDP-225		27-2/137-140	ch	Petrichenko		217	968			271				71.8	8.1	20.1	
sw	DSDP-225		28-1/062-066	ch	Petrichenko		257	1177			274				74.5	8.1	17.3	
					Miocene, Messinian: Mediterranean Sea (Ayora et al., 1994b; Garçia-Veigas et al., 1995; Zimmermann, 2000b)													
sw	Porto-E-38	LU	647	ch	SEM-EDS	2470	520	2150		6190	550			0.0	72.6	8.8	18.6	
sw	Siculiana-1	LU	745	ch	SEM-EDS	2620	460	2480		6880	580			0.0	75.4	7.0	17.6	
sw	Siculiana-1	LU	675	ch	SEM-EDS	2200	470	2500		6490	590			0.0	75.2	7.1	17.7	
sw	Siculiana-1	LU	647	ch	SEM-EDS	1360	610	3250		7030	720			0.0	76.0	7.1	16.8	
sw	Realmonte	LU	3′	ch	SEM-EDS	2430	460	2210		6230	540			0.0	74.2	7.7	18.1	
sw	Porto-E.-38	UU	340	ch	SEM-EDS	4420	230	800		5790	230			0.0	69.9	10.0	20.1	
sw	Realmonte	UU	13	ch	SEM-EDS	4210	250	1130		6100	310			0.0	72.2	8.0	19.8	
sw	Realmonte	UU	SRe95-14/04	ch	LA-ICP-MS/SEM-EDS	4770	170	820	10	6050	230	16.5		1.4	72.9	7.6	19.6	
sw	Realmonte	UU	SRe95-14/06	ch	LA-ICP-MS/SEM-EDS	4690	220	1030	10	5740	310			9.4	71.5	7.6	20.8	
sw	Lorca-S5	LHU	127	ch	SEM-EDS	3170	380	1540		5620	490			0.5	69.4	8.6	22.1	
sw	Lorca-S5	LHU	134	ch	SEM-EDS	3630	360	1390		5680	440			3.2	69.2	9.0	21.9	
					Miocene, Badenian: Forecarpathian B., Eastern Europe (Kovalevich and Petrichenko, 1997; Galamay and Karoli, 1997; Galamay et al., 1997; Garçia-Veigas et al., 1997)													
sw	FCB	Wieliczka	breccia	ch	Petrichenko		144	818			136				79.7	7.0	13.2	
sw*	FCB	Wieliczka	spiza salt	ch	Petrichenko		155	918			184				77.8	6.6	15.6	
sw*	FCB	Wieliczka	spiza salt	ch	Petrichenko		274	1195			193				78.4	9.0	12.7	
sw*	FCB	Wieliczka	shaft salt	ch	Petrichenko		226	945			130				79.6	9.5	10.9	
sw*	FCB	Wieliczka	green salt	ch	Petrichenko		263	877			201				72.5	10.9	16.6	
sw*	FCB	Wieliczka	105	ch	Petrichenko		172	813			160				76.8	8.1	15.1	
sw*	FCB	Wieliczka	106	ch	Petrichenko		169	804			123				79.5	8.4	12.2	
sw*	FCB	Wieliczka	107	ch	Petrichenko		155	809			118				80.5	7.7	11.8	
sw*	FCB	Wieliczka	16	ch	Petrichenko		184	863			138				79.0	8.4	12.6	

(Continued)

Appendix. (Continued)

	Stratigraphy/basin		Sample	Inclusion type	Method	Na	K	Mg	Ca	Cl	SO_4	Br	Li	CB	Mg	2K	SO_4	Ca
						(mmol/kg H_2O)								(%)	Jänecke unit (%)			
Miocene, Badenian: Forecarpathian B., Eastern Europe (Kovalevich and Petrichenko, 1997; Galamay and Karoli, 1997; Galamay et al., 1997; Garçia-Veigas et al., 1997)																		
sw	FCB	Wieliczka	120	ch	Petrichenko		169	909			116				81.9	7.6	10.5	
sw*	FCB	Wieliczka	118	ch	Petrichenko		217	890			140				78.1	9.5	12.3	
sw*	FCB	Wieliczka	117	ch	Petrichenko		206	904			117				80.4	9.2	10.4	
sw*	FCB	Wieliczka	98	ch	Petrichenko		212	850			118				79.1	9.9	11.0	
sw*	FCB	Wieliczka	100	ch	Petrichenko		212	850			129				78.4	9.8	11.9	
sw*	FCB	Wieliczka	99	ch	Petrichenko		155	827			128				80.1	7.5	12.4	
sw	FCB	Wieliczka	6	ch	Petrichenko		147	804			147				78.5	7.2	14.4	
sw	FCB	Wieliczka	87	ch	Petrichenko		147	854			131				80.7	6.9	12.4	
sw*	FCB	Wieliczka	91	ch	Petrichenko		209	1013			131				81.1	8.4	10.5	
sw*	FCB	Wieliczka	89	ch	Petrichenko		206	1022			143				80.6	8.1	11.2	
sw	FCB	Wieliczka	12	ch	Petrichenko		147	854			133				80.5	6.9	12.6	
sw	FCB	Wieliczka	10	ch	Petrichenko		158	909			143				80.4	7.0	12.6	
sw	FCB	Wieliczka	20	ch	Petrichenko		138	772			152				77.8	7.0	15.3	
sw*	ESB	Zbudza	Ep-2, 238.4	ch	Petrichenko		153	804			161				77.2	7.3	15.5	
sw	ESB	Zbudza	Ep-2, 239.2	ch	Petrichenko		147	786			157				77.3	7.2	15.5	
sw*	ESB	Zbudza	Ep-2, 71	ch	Petrichenko		144	631			100				78.6	9.0	12.4	
sw*	ESB	Zbudza	Ep-2, 70	ch	Petrichenko		136	609			101				78.3	8.7	13.0	
sw*	ESB	Zbudza	Ep-2, 68	ch	Petrichenko		110	591			98				79.4	7.4	13.1	
sw*	ESB	Zbudza	Ep-2, 65	ch	Petrichenko		155	759			105				80.6	8.3	11.1	
sw*	ESB	Zbudza	Ep-2, 63	ch	Petrichenko		147	586			108				76.4	9.6	14.1	
sw*	ESB	Zbudza	Ep-2, 61	ch	Petrichenko		127	518			95				76.5	9.4	14.1	
sw*	ESB	Zbudza	Ep-2, 59	ch	Petrichenko		121	613			99				79.4	7.9	12.8	
sw*	ESB	Zbudza	Ep-2, 57	ch	Petrichenko		136	581			103				77.3	9.0	13.7	
sw*	ESB	Zbudza	Ep-2, 56	ch	Petrichenko		144	563			101				76.5	9.8	13.7	
sw*	ESB	Zbudza	Ep-2, 55	ch	Petrichenko		147	591			113				76.0	9.5	14.5	
sw*	ESB	Zbudza	Ep-2, 54	ch	Petrichenko		133	550			99				76.9	9.3	13.8	
sw*	ESB	Zbudza	Ep-2, 53	ch	Petrichenko		127	604			111				77.5	8.2	14.3	
sw*	ESB	Zbudza	Ep-2, 52	ch	Petrichenko		127	572			110				76.7	8.5	14.8	
sw	ESB	Zbudza	Ep-2, 50	ch	Petrichenko		93	500			94				78.0	7.3	14.7	
Oligocene: Mulhouse Basin, France (Canals et al., 1993)																		
sw*	MB	Salt IV	19.79	ch		2280	481	1604	117	6370	36			−3.8	83.3	12.5		4.2
sw*	MB	Salt IV	20.50	ch		3024	369	1187	43	5402	60			5.8	85.5	13.3	1.3	
Eocene: Navarra Basin, North Spain (Ayora et al., 1994a)																		
sw*	NB	Biurrun	BI-425	ch	SEM-EDS	2640	560	1870		6570	160			0.7	81.0	12.1	6.9	
sw*	NB	Biurrun	BI-430	ch	SEM-EDS	2580	520	1650		6640	120			−7.2	81.3	12.8	5.9	
sw*	NB	Biurrun	BI-436	ch	SEM-EDS	2730	400	1690		6590	150			−5.7	82.8	9.8	7.4	
sw*	NB	Biurrun	BI-437	ch	SEM-EDS	3680	360	1360		6910	140			−6.2	81.0	10.7	8.3	
Upper Jurassic, Kimmeridgian: Kongazsky Series, Predobrogea Basin (Khmelevska, 1997)																		
sw*	U. Jurassic	Kimmeridge	R65	ch	Petrichenko		159	422	207						59.6	11.2		29.2
Upper Jurassic, Kimmeridgian: Haynesville Formation, Gulf Coast (this study)																		
	U. Jurassic	Haynesville-Form.	10178-1		Extraction-IC	983	332	2365	909	8073		47.5	6.6	−2.7	68.8	4.8		26.4
	U. Jurassic	Haynesville-Form.	10178-2		Extraction-IC	980	240	2401	948	7714		29.5	6.2	2.6	69.2	3.5		27.3
	U. Jurassic	Haynesville-Form.	10178-3		Extraction-IC	810	144	2447	1129	8682		45.8		−6.9	67.1	2.0		30.9
	U. Jurassic	Haynesville-Form.	10178-4		Extraction-IC	921	288	2450	942	8023		50.8		−0.4	69.3	4.1		26.7

(Continued)

Appendix. (Continued)

Stratigraphy/basin		Sample	Inclusion type	Method	Na	K	Mg	Ca	Cl	SO_4	Br	Li	CB	Mg	2K	SO_4	Ca
					(mmol/kg H_2O)								(%)	Jänecke unit (%)			
Upper Jurassic, Kimmeridgian: Haynesville Formation, Gulf Coast (this study)																	
U. Jurassic	Haynesville-Form.	10178-5		Extraction-IC	1242	272	2257	906	7894		39.1		−0.7	68.4	4.1		27.5
U. Jurassic	Haynesville-Form.	10178-6		Extraction-IC	771	398	2547	979	8358		56.7		−1.7	68.4	5.3		26.3
U. Jurassic	Haynesville-Form.	10333-1		Extraction-IC	476	487	3038	1167	9404		46.6	4.9	−0.3	68.3	5.5		26.2
U. Jurassic	Haynesville-Form.	10333-2		Extraction-IC	559	473	2926	1086	9139		49.3	3.5	−0.9	68.9	5.6		25.6
U. Jurassic	Haynesville-Form.	10333-3		Extraction-IC	589	610	2878	1048	9416		52.4	6.8	−3.9	68.0	7.2		24.8
U. Jurassic	Haynesville-Form.	10333-4		Extraction-IC	879	587	2559	894	8464		53.7	8.3	−1.1	68.3	7.8		23.9
U. Jurassic	Haynesville-Form.	10333-5		Extraction-IC	694	507	2815	1173	9054		48.4		1.4	66.4	6.0		27.7
U. Jurassic	Haynesville-Form.	10896-1		Extraction-IC	2942	368	957	762	6940		22.4		−2.8	50.3	9.7		40.0
U. Jurassic	Haynesville-Form.	10896-2		Extraction-IC	3276	290	1233	478	6394		15.8		8.9	66.4	7.8		25.8
U. Jurassic	Haynesville-Form.	10896-3		Extraction-IC	2863	347	1186	675	6750		17.1		2.7	58.3	8.5		33.2
Middle Jurassic: Louann Formation, Gulf Coast (Land et al., 1995)																	
M. Jurassic	Louann-Formation	11355-1	ch	Extraction-IC	1460	983	1770	867	8300		67.5	17	−7.3	56.6	15.7		27.7
M. Jurassic	Louann-Formation	11355-2	ch	Extraction-IC	1679	1184	1955	745	7898		59.9	28	4.5	59.4	18.0		22.6
M. Jurassic	Louann-Formation	11355-3	ch	Extraction-IC	1914	1245	1486	929	8031		58.0	25	−0.5	48.9	20.5		30.6
M. Jurassic	Louann-Formation	11364-1	ch	Extraction-IC	1145	942	2535	744	8088		41.5	14	1.9	65.8	13.3		20.9
M. Jurassic	Louann-Formation	11364-2	ch	Extraction-IC	1139	943	2391	806	8272		79.6	12	2.4	65.2	12.9		22.0
M. Jurassic	Louann-Formation	11364-3	ch	Extraction-IC	1131	946	2349	783	8302		45.6	14	0.5	65.2	13.1		21.7
M. Jurassic	Louann-Formation	11364-4	ch	Extraction-IC	1176	988	2251	899	8113		89.0	11	4.2	61.8	13.6		24.7
M. Jurassic	Louann-Formation	11364-5	ch	Extraction-IC	1005	889	2347	845	7923		86.7	15	4.4	64.5	12.2		23.2
M. Jurassic	Louann-Formation	11440-1	ch	Extraction-IC	1867	1112	1432	856	7595		53.9	19	−0.5	50.3	19.5		30.1
M. Jurassic	Louann-Formation	11440-2	ch	Extraction-IC	1660	1090	1630	866	8170		56.0	27	−5.4	53.6	17.9		28.5
M. Jurassic	Louann-Formation	11440-3	ch	Extraction-IC	1492	1033	1467	920	7799		62.2	27	−6.6	50.5	17.8		31.7
M. Jurassic	Louann-Formation	11440-4	ch	Extraction-IC	1919	1268	1479	922	7852		58.2	28	1.7	48.7	20.9		30.4
Late Triassic-Early Jurassic: Offshore Morocco, DSDP Leg 79, Site 546 (this study)																	
E. Jurassic	Rhaet-Hettangian	79-546-1	ch	Extraction-IC	150	79	3410	1960	10600		92.8		3.4	63.0	0.7		36.2
E. Jurassic	Rhaet-Hettangian	79-546-2	ch	Extraction-IC	177	106	3600	2150	11000		111	13	6.9	62.0	0.9		37.0
E. Jurassic	Rhaet-Hettangian	79-546-3	ch	Extraction-IC	268	191	2390	2590	10200		95.8	28	2.1	47.1	1.9		51.0
E. Jurassic	Rhaet-Hettangian	79-546-4	ch	Extraction-IC	255	168	2940	2790	11400		119	29	4.1	50.6	1.4		48.0
E. Jurassic	Rhaet-Hettangian	79-546-6	ch	Extraction-IC	127	136	2430	3270	11700		46.0		−0.3	42.1	1.2		56.7
Upper Triassic, Early Carnesian: Lorraine Basin, borehole SG26 (Fanlo and Ayora, 1998)																	
Keuper	SG26-226.7	P-H40	ch	SEM-EDS	2350	90	2020		7080	60			−1.3	95.1	2.1	2.8	
Keuper	SG26-220.4	P-H39	ch	SEM-EDS	2210	490	2310		7000	160			−7.4	85.1	9.0	5.9	
Keuper	SG26-220.8	P-H38	ch	SEM-EDS	2410	120	2060		6930	50			−5.1	94.9	2.8	2.3	
Keuper	SG26-225.6	P-H34	ch	SEM-EDS	2290	120	2090		7190	240			−1.7	87.4	2.5	10.0	
Keuper	SG26-226.3	P-H32	ch	SEM-EDS	2430	330	2000		7000	240			−6.7	83.2	6.9	10.0	
Keuper	SG26-232.3	P-H28	ch	SEM-EDS	2310	190	2160		6960	110			−8.5	91.3	4.0	4.7	
Keuper	SG26-232.8	P-H27	ch	SEM-EDS	2540	180	1990		6900	260			−10.3	85.0	3.8	11.1	
Keuper	SG26-240.0	P-H23	ch	SEM-EDS	2270	260	2130		7140	140			−2.5	88.8	5.4	5.8	
Keuper	SG26-243.1	P-H21	ch	SEM-EDS	1970	520	2380		7530	70			−5.5	87.8	9.6	2.6	
Keuper	SG26-270.0	N-H17	ch	SEM-EDS	1870	170	2430		7330	50			−3.2	94.7	3.3	1.9	
Keuper	SG26-277.9	N-H14	ch	SEM-EDS	2500	210	1810		7320	30			0.7	93.1	5.4	1.5	
Keuper	SG26-278.8	N-H13	ch	SEM-EDS	1950	120	2420		7100	40			−7.2	96.0	2.4	1.6	
Keuper	SG26-280.5	N-H11	ch	SEM-EDS	2670	100	1960		6610	50			−13.9	95.1	2.4	2.4	
Keuper	SG26-283.9	N-H9	ch	SEM-EDS	1690	120	2590		7540	40			−5.7	96.3	2.2	1.5	
Keuper	SG26-285.1	N-H8	ch	SEM-EDS	2580	90	1840		7120	70			−6.2	94.1	2.3	3.6	

(Continued)

Appendix. (Continued)

	Stratigraphy/basin		Sample	Inclusion type	Method	Na	K	Mg	Ca	Cl	SO_4	Br	Li	CB (%)	Mg	2K	SO_4	Ca
						(mmol/kg H_2O)									Jänecke unit (%)			
	Upper Triassic, Early Carnesian: Lorraine Basin, borehole SG26 (Fanlo and Ayora, 1998)																	
	Keuper	SG26-285.3	N-H7	ch	SEM-EDS	2320	160	2000		7230	30			−3.0	94.8	3.8	1.4	
	Keuper	SG26-285.9	N-H6	ch	SEM-EDS	2350	230	2050		7040	30			−0.9	93.4	5.2	1.4	
	Keuper	SG26-289.0	N-H4	ch	SEM-EDS	2340	70	2010		7180	50			−3.7	95.9	1.7	2.4	
	Keuper	SG26-291.2	N-H1	ch	SEM-EDS	2190	240	2210		7120	180			0.5	88.0	4.8	7.2	
	Upper Triassic, Early Carnesian: Lorraine Basin, Varangeville (this study)																	
	Keuper	Varangeville	1-1	ch	Extraction-IC	2130	225	2303		6742	69	53.7		1.2	92.7	4.5	2.8	
	Keuper	Varangeville	1-2	ch	Extraction-IC	2478	272	2122	18	7087	96	55.7		−3.5	90.8	5.8	3.3	
	Keuper	Varangeville	1-3	ch	Extraction-IC	1918	170	2534	98	7162	7	70.0		2.4	93.5	3.1		3.4
	Keuper	Varangeville	1-4	ch	Extraction-IC	2181	244	2250	20	6814	70	60.1		0.2	92.9	5.0	2.1	
	Keuper	Varangeville	1-5	ch	Extraction-IC	1967	190	2310		6407	67	68.0		3.5	93.4	3.8	2.7	
	Keuper	Varangeville	1-6	ch	Extraction-IC	2160	286	2281	21	6788	47	54.6		2.4	93.1	5.8	1.1	
	Keuper	Varangeville	1-7	ch	Extraction-IC	1817	136	2538		6809	98	69.7		0.4	93.9	2.5	3.6	
	Keuper	Varangeville	2-1	ch	Extraction-IC	1872	172	2635		7398	55	63.9		−2.6	94.9	3.1	2.0	
	Keuper	Varangeville	2-2	ch	Extraction-IC	2265	191	1897		6238	40	51.2		−1.1	93.4	4.7	1.9	
sw*	Keuper	Varangeville	2-3	ch	Extraction-IC	2832	541	1658		6605	35	50.7		0.2	84.4	13.8	1.8	
	Keuper	Varangeville	2-4	ch	Extraction-IC	3140	262	1640	34	6204	43	44.4		7.1	92.1	7.4	0.5	
	Keuper	Varangeville	3-1	ch	Extraction-IC	1652	654	2411	34	7279	15	81.6		−1.6	87.5	11.9		0.7
	Keuper	Varangeville	3-2	ch	Extraction-IC	2530	645	2012	28	6631	38	64.2		7.8	85.8	13.8	0.4	
	Keuper	Varangeville	3-3	ch	Extraction-IC	1810	629	2228	73	6977	14	74.3		0.5	85.7	12.1	2.2	
	Keuper	Varangeville	3-4	ch	Extraction-IC	1921	527	2368	31	7144	20	79.8		0.9	89.6	10.0		0.4
	Middle Triassic, Lower Anisian: Muschelkalk Basin, N Switzerland (Kovalevich and Hauber, 2000)																	
sw*	Muschelkalk	R65	198.2m	ch	Petrichenko		216	651			73				78.3	13.0	8.7	
sw?	Muschelkalk	S129	395.7m	ch	Petrichenko		319	674			79				78.6	14.3	7.1	
	Upper Permian: Leine Formation, Allertalgraben, Bartensleben, Germany (Herrmann et al., 1997)																	
	Zechstein 3	Na3β, 55. L.	1-1		Extraction-IC	2664	527	1063	43	5301	52	23.6	3.8	0.0	79.6	19.8	0.6	
	Zechstein 3	Na3γ, 200. L.	2-1		Extraction-IC	2609	389	1832	22	6439	133	32.7	3.9	0.0	85.7	9.1	5.2	
	Zechstein 3	Na3γ, 200. L.	2-2		Extraction-IC	2720	372	1676	18	6200	140	30.1	3.9	0.0	84.5	9.4	6.2	
	Zechstein 3	Na3γ, 200. L.	2-3		Extraction-IC	2331	455	1549	9	5340	281	28.6	3.8	0.0	75.6	11.1	13.3	
sw	Zechstein 3	Na3γ, 200. L.	2-4		Extraction-IC	2609	328	1538	44	5490	305	27.4	3.8	0.0	78.4	8.3	13.3	
sw	Zechstein 3	Na3γ, 200. L.	2-5		Extraction-IC	2220	278	1421	61	4940	261	23.3	3.7	0.0	80.8	7.9	11.4	
sw	Zechstein 3	Na3γ, 200. L.	2-6		Extraction-IC	3053	400	2387	89	7449	477	34.7	8.1	0.0	80.2	6.7	13.1	
sw	Zechstein 3	Na3γ, 195. L.	3-1		Extraction-IC	2553	333	1649	4	5551	320	27.4	3.8	0.0	77.3	7.8	14.8	
sw	Zechstein 3	Na3γ, 195. L.	3-2		Extraction-IC	2553	333	1699	23	5662	334	28.1	3.8	0.0	78.1	7.7	14.3	
sw	Zechstein 3	Na3γ, 195. L.	3-3		Extraction-IC	2387	300	1560	9	5240	292	25.6	3.7	0.0	78.3	7.5	14.2	
	Zechstein 3	Na3γ, 195. L.	3-4		Extraction-IC	1388	339	2798	27	7055	160	46.9	12	0.0	90.2	5.5	4.3	
sw	Zechstein 3	Na3γ, 195. L.	3-5		Extraction-IC	1277	555	3231	21	7272	532	38.9	5.9	0.0	80.4	6.9	12.7	
sw	Zechstein 3	Na3γ, 195. L.	3-6		Extraction-IC	3553	433	2115	7	7427	401	32.8	6.1	0.0	77.6	7.9	14.5	
	Zechstein 3	Na3γ, 195. L.	4-1		Extraction-IC	2109	555	2260	45	7105	84	32.4	4.0	0.0	87.7	10.8	1.5	
	Zechstein 3	Na3γ, 195. L.	4-2		Extraction-IC	2387	555	2344	33	7605	46	38.4	4.0	0.0	89.0	10.5	0.5	
	Upper Permian: Boulby Formation, England (this study)																	
	Zechstein 3		1		Extraction-IC	503	629	3170	494	8780		55.5	37	−3.7	79.7	7.9		12.4
	Zechstein 3		2		Extraction-IC	490	633	3330	531	8300		63.0	25	6.4	79.7	7.6		12.7

(Continued)

Appendix. (Continued)

	Stratigraphy/basin	Sample	Inclusion type	Method	Na	K	Mg	Ca	Cl	SO_4	Br	Li	CB (%)	Mg	2K	SO_4	Ca
					(mmol/kg H_2O)									Jänecke unit (%)			
				Upper Permian: Boulby Formation, England (this study)													
	Zechstein 3	3		Extraction-IC	649	788	2830	898	8700		71.1	32	2.2	68.7	9.6		21.8
	Zechstein 3	4		Extraction-IC	627	770	2470	1360	9084		63.4	32	−0.3	58.6	9.1		32.3
	Zechstein 3	5		Extraction-IC	533	637	3670	226	8600		61.7	22	4.1	87.1	7.6		5.4
				Upper Permian: Delaware Basin, Rustler Formation (this study)													
	Rustler Formation	H11-1		Extraction-IC	449	526	3870		8640	33	24.9		0.1	92.9	6.3	0.8	
	Rustler Formation	H11-2		Extraction-IC	222	159	4680		9230	4	169	34	5.3	98.3	1.7	0.1	
	Rustler Formation	H11-3		Extraction-IC	274	172	4430		9020	12	179	41	2.9	97.8	1.9	0.3	
	Rustler Formation	H11-4		Extraction-IC	476	547	3960		8800	60	38.4	9.2	0.3	92.2	6.4	1.4	
	Rustler Formation	W19-1		Extraction-IC	445	406	4200		8470	63	48.8	10	7.3	94.0	4.5	1.4	
	Rustler Formation	W19-2		Extraction-IC	464	613	3990	227	9660		31.7		−1.6	88.2	6.8		5.0
	Rustler Formation	W19-3		Extraction-IC	878	196	2990	463	7510		51.8		6.1	84.2	2.8		13.0
	Rustler Formation	H12-1		Extraction-IC	1460	1070	1830	782	7530		38.1		2.9	58.2	17.0		24.8
	Rustler Formation	H12-2		Extraction-IC	1070	655	2800	362	7760		61.3	5.5	3.7	80.2	9.4		10.4
	Rustler Formation	H12-3		Extraction-IC	1030	495	2600	588	7570		62.0	5.8	4.3	75.7	7.2		17.1
	Rustler Formation	H12-4		Extraction-IC	1530	1140	2360	505	8130		53.5		3.3	68.7	16.6		14.7
				Upper Permian: Delaware Basin, Salado Formation (Horita et al., 1991)													
sw*	Ochoan/Salado	WIPP-3: basal	ch	Extraction-IC	5120	132	575		6040	145	12.6		1.1	73.2	8.4	18.4	
sw*	Ochoan/Salado	WIPP-3: basal	ch	Extraction-IC	4960	119	647		6040	155	12.0	1	0.4	75.1	6.9	18.0	
	Ochoan/Salado	WIPP-3: basal	ch	Extraction-IC	4770	125	772		6180	177	16.4		−1.5	76.3	6.2	17.5	
	Ochoan/Salado	WIPP-3: basal	ch	Extraction-IC	4830	96.4	785	16	6020	181	15.7	5	2.3	78.6	4.8	16.5	
	Ochoan/Salado	WIPP-3: basal	ch	Extraction-IC	4170	123	1250		6280	276	20.0		−0.6	78.7	3.9	17.4	
	Ochoan/Salado	WIPP-3: basal	ch	Extraction-IC	4170	149	1260		6060	307	16.4		2.4	76.8	4.5	18.7	
sw*	Ochoan/Salado	WIPP-4: 655.3 m	ch	Extraction-IC	2480	480	2080		6200	406	39.4		1.5	76.3	8.8	14.9	
sw*	Ochoan/Salado	WIPP-4: 655.3 m	ch	Extraction-IC	2680	476	2150		6590	459	37.2		−0.7	75.5	8.4	16.1	
sw*	Ochoan/Salado	WIPP-4: 655.3 m	ch	Extraction-IC	2540	481	2160		6440	428	34.0	3	0.6	76.4	8.5	15.1	
sw*	Ochoan/Salado	WIPP-4: 655.3 m	ch	Extraction-IC	2480	433	2170		6480	422	34.1		−1.0	77.3	7.7	15.0	
sw*	Ochoan/Salado	WIPP-4: 655.3 m	ch	Extraction-IC	2490	449	2190		6330	416	34.7		2.2	77.4	7.9	14.7	
sw*	Ochoan/Salado	WIPP-4: 655.3 m	ch	Extraction-IC	2510	451	2200		6130	400	31.3	5	6.0	77.9	8.0	14.2	
sw*	Ochoan/Salado	WIPP-4: 655.3 m	ch	Extraction-IC	2510	469	2200		6540	428	37.0		−0.2	76.9	8.2	15.0	
sw*	Ochoan/Salado	WIPP-4: 655.3 m	ch	Extraction-IC	2460	466	2200		6500	427	34.4		−0.4	76.9	8.1	14.9	
sw*	Ochoan/Salado	WIPP-4: 655.3 m	ch	Extraction-IC	2490	474	2210		6390	427	33.7	2	1.9	76.9	8.2	14.9	
sw*	Ochoan/Salado	WIPP-4: 655.3 m	ch	Extraction-IC	2510	460	2210		6520	430	34.1		0.1	77.0	8.0	15.0	
sw*	Ochoan/Salado	WIPP-4: 655.3 m	ch	Extraction-IC	2170	443	2240		6590	421	34.9		−4.7	77.7	7.7	14.6	
sw*	Ochoan/Salado	WIPP-4: 655.3 m	ch	Extraction-IC	2590	491	2260		6590	426	36.9		2.1	77.1	8.4	14.5	
sw*	Ochoan/Salado	WIPP-4: 655.3 m	ch	Extraction-IC	2330	443	2270		6380	423	34.6		1.2	77.9	7.6	14.5	
sw*	Ochoan/Salado	WIPP-4: 655.3 m	ch	Extraction-IC	2440	464	2290		6440	437	34.7		2.3	77.4	7.8	14.8	
sw*	Ochoan/Salado	WIPP-4: 655.3 m	ch	Extraction-IC	2460	494	2340		6340	423	34.3		6.0	77.7	8.2	14.1	
sw*	Ochoan/Salado	WIPP-4: 655.3 m	ch	Extraction-IC	2500	469	2390		6530	427	35.8	2	4.8	78.3	7.7	14.0	
	Ochoan/Salado	WIPP-4: 655.3 m	ch	Extraction-IC	2060	418	2520		6530	405	36.4	3	2.4	80.4	6.7	12.9	
	Ochoan/Salado	WIPP-4: 655.3 m	ch	Extraction-IC	1920	397	2590		6370	397	36.1	3	4.5	81.3	6.2	12.5	
				Upper Permian: Werra Formation, Poland (Peryt and Kovalevich, 1996)													
sw	Zechstein 1	Zdrada IG3, 7	ch	Petrichenko		230	1224			161				81.6	7.7	10.7	
	Zechstein 1	Zdrada IG3, 3	ch	Petrichenko		220	1627			194				84.2	5.7	10.1	
	Zechstein 1	Zdrada IG6, 29a	ch	Petrichenko		269	1555			248				80.2	6.9	12.8	
sw	Zechstein 1	Zdrada IG6, 28a	ch	Petrichenko		188	1023			176				79.1	7.3	13.6	

(Continued)

Appendix. (Continued)

	Stratigraphy/basin		Sample	Inclusion type	Method	Na	K	Mg	Ca	Cl	SO_4	Br	Li	CB	Mg	2K	SO_4	Ca
						(mmol/kg H_2O)								(%)	Jänecke unit (%)			
	Upper Permian: Werra Formation, Poland (Peryt and Kovalevich, 1996)																	
	Zechstein 1		Zdrada IG6, 27a	ch	Petrichenko		65	445			96				77.6	5.7	16.7	
	Zechstein 1		Zdrada IG6, 26a	ch	Petrichenko		208	1212			181				81.0	6.9	12.1	
	Zechstein 1		Zdrada IG6, 25	ch	Petrichenko		239	1519			224				81.6	6.4	12.0	
sw	Zechstein 1		Zdrada IG6, 30a	ch	Petrichenko		235	970			162				77.6	9.4	13.0	
	Zechstein 1		Zdrada IG6, 23	ch	Petrichenko		112	678			146				77.0	6.4	16.6	
	Zechstein 1		Zdrada IG6, 19	ch	Petrichenko		128	733			134				78.7	6.9	14.4	
	Zechstein 1		Zdrada IG6, 16	ch	Petrichenko		129	927			171				79.7	5.5	14.7	
	Zechstein 1		Zdrada IG6, 12	ch	Petrichenko		165	1176			179				81.9	5.7	12.4	
sw	Zechstein 1		Zdrada IG6, 8	ch	Petrichenko		228	1109			212				77.2	8.0	14.8	
	Zechstein 1		Zdrada IG6, 3	ch	Petrichenko		115	1063			142				84.2	4.5	11.2	
sw	Zechstein 1		Zdrada IG8, 19	ch	Petrichenko		147	573			126				74.2	9.5	16.3	
	Zechstein 1		Zdrada IG8, 12	ch	Petrichenko		114	759			172				76.8	5.8	17.4	
sw	Zechstein 1		Zdrada IG8, 16	ch	Petrichenko		208	831			178				74.7	9.3	16.0	
sw	Zechstein 1		Zdrada IG8, 7	ch	Petrichenko		187	1014			193				78.0	7.2	14.8	
sw	Zechstein 1		Zdrada IG8, 4	ch	Petrichenko		163	843			185				75.9	7.4	16.7	
	Lower Permian: Kansas Basin, Wellington Formation, Hutchinson Salt Member (Horita et al., 1991)																	
sw*	Leonardian	We-2: ASC mine	1	ch	Extraction-IC	3080	347	1600	12	6030	262	29.2	2	1.5	79.1	8.6	12.4	
	Leonardian	We-2: ASC mine	3	ch	Extraction-IC	2330	353	2200		6770	272	42.4	4	−3.2	83.1	6.7	10.3	
	Leonardian	We-1: 198.1m	3		Extraction-IC	2900	401	1780		6600	100	34.9		0.9	85.6	9.6	4.8	
	Leonardian	We-1: 198.1m	1		Extraction-IC	2710	364	1800		6320	98	33.9		2.4	86.5	8.8	4.7	
	Leonardian	We-1: 198.1m	5		Extraction-IC	2710	270	1810		6980	23	22.8		−6.2	92.0	6.9	1.2	
	Leonardian	We-1: 198.1m	12		Extraction-IC	2670	243	1820		6430	17	38.0		1.4	92.9	6.2	0.9	
	Leonardian	We-1: 198.1m	4		Extraction-IC	2490	387	2090		6620	103	38.8		3.3	87.6	8.1	4.3	
	Leonardian	We-1: 198.1m	8		Extraction-IC	2280	455	2280		7020	130	43.5		0.2	86.4	8.6	4.9	
	Leonardian	We-1: 198.1m	2		Extraction-IC	1830	207	2470		6850	16	41.9		1.4	95.4	4.0	0.6	
	Leonardian	We-1: 198.1m	10		Extraction-IC	1790	409	2530		7040	134	45.6		−0.7	88.2	7.1	4.7	
	Leonardian	We-1: 198.1m	11		Extraction-IC	1480	379	2760		6900	173	51.3		1.8	88.4	6.1	5.5	
	Leonardian	We-1: 198.1m	6		Extraction-IC	1590	375	2780		7060	141	48.8		2.5	89.4	6.0	4.5	
	Leonardian	We-1: 198.1m	9		Extraction-IC	1350	325	3080		7610	122	57.3		−0.2	91.5	4.8	3.6	
	Leonardian	We-1: 198.1m	7		Extraction-IC	1060	327	3230		7500	128	60.4		1.2	91.7	4.6	3.6	
	Middle Devonian: Saskatchewan Basin, Prairie Formation, Elk Point Group (Horita et al., 1996)																	
	Saskatchewan	IMC K-1	AW30-F2		Extraction-IC	83	53	2960	3270	11900		49.8	7	5.7	47.3	0.4		52.3
	Saskatchewan	IMC K-1	AW30-F4		Extraction-IC	172	44	2590	2890	10200		47.0	6	9.1	47.1	0.4		52.5
	Saskatchewan	IMC K-1	AW30-F11		Extraction-IC	72	60	2960	3460	12600		58.3	6	2.9	45.9	0.5		53.6
	Saskatchewan	IMC K-1	AW30-F11		Extraction-IC	74	41	2940	3470	12400		55.8	6	4.2	45.7	0.3		54.0
	Saskatchewan	IMC K-1	AW32-F5		Extraction-IC	83	43	2910	3090	11400		52.7	6	6.2	48.3	0.4		51.3
	Saskatchewan	IMC K-1	AW38-F1		Extraction-IC	88	43	2830	3200	11200		51.4	6	8.5	46.8	0.4		52.9
	Saskatchewan	IMC K-1	AW38-F2		Extraction-IC	109	62	2820	3340	11300		54.2	6	10.0	45.5	0.5		53.9
	Saskatchewan	IMC K-1	AW40B-F1		Extraction-IC	79	35	2980	3200	12400		56.8	6	0.6	48.1	0.3		51.6
	Saskatchewan	IMC K-1	AW40B-F3		Extraction-IC	101	51	2700	3190	10900		50.9	4	9.0	45.6	0.4		53.9
	Saskatchewan	IMC K-1	AW40B-F4		Extraction-IC	75	29	2960	3210	11500		54.1	7	7.9	47.9	0.2		51.9
	Saskatchewan	IMC K-1	AW40B-F5		Extraction-IC	72	32	2980	3240	12400		58.1	7	1.2	47.8	0.3		52.0
sw?	Saskatchewan	Lanigan	AW46-F4	ch	Extraction-IC	3480	377	1060	440	6380		25.0		7.2	62.8	11.2		26.1
	Saskatchewan	Lanigan	AW46-F11	ch	Extraction-IC	2970	240	1170	470	6430		24.5		0.9	66.5	6.8		26.7
	Saskatchewan	Lanigan	AW46-F14	ch	Extraction-IC	3060	229	1240	453	6710		24.9		−0.5	68.6	6.3		25.1

(Coninued)

Appendix. (Continued)

	Stratigraphy/basin		Sample	Inclusion type	Method	Na	K	Mg	Ca	Cl	SO_4	Br	Li	CB (%)	Mg	2K	SO_4	Ca
						(mmol/kg H_2O)									Jänecke unit (%)			
					Middle Devonian: Saskatchewan Basin, Prairie Formation, Elk Point Group (Horita et al., 1996)													
	Saskatchewan	Lanigan	AW47-F4		Extraction-IC	85	55	2020	4140	12300		56.6	6	1.3	32.6	0.4		66.9
	Saskatchewan	Bredenbury	AW49-F7		Extraction-IC	953	121	1720	2050	7660		30.7	3	11.7	44.9	1.6		53.5
	Saskatchewan	Bredenbury	AW49-F13		Extraction-IC	172	137	2220	3290	10600		57.6	7	6.6	39.8	1.2		59.0
	Saskatchewan	Bredenbury	AW49-F27		Extraction-IC	933	94	1650	2010	8170		33.2	5	2.1	44.5	1.3		54.2
	Saskatchewan	Bredenbury	AW49-F28		Extraction-IC	145	115	2810	3440	11700		52.9	6	8.7	44.6	0.9		54.5
	Saskatchewan	Bredenbury	AW49-F21	ch	Extraction-IC	1880	68	1730	711	6540		34.7		4.3	69.9	1.4		28.7
	Saskatchewan	Bredenbury	AW49-F22	ch	Extraction-IC	2200	47	1210	1190	6750		12.6		4.3	49.9	1.0		49.1
	Saskatchewan	Bredenbury	AW49-F23	ch	Extraction-IC	1910	44	1940	568	6940		14.2		0.4	76.7	0.9		22.5
	Saskatchewan	Bredenbury	AW49-F24	ch	Extraction-IC	1920	56	1900	670	7060		12.5		0.8	73.1	1.1		25.8
	Saskatchewan	Bredenbury	AW49-F25	ch	Extraction-IC	2180	121	1230	1180	6790		41.0		4.8	49.8	2.4		47.8
sw*	Saskatchewan	Bredenbury	AW49-F26	ch	Extraction-IC	3170	262	808	674	6560		22.6		−2.5	50.1	8.1		41.8
					Late Silurian: Michigan Basin, Salina Group, F Salt 1 (Das et al., 1990)													
	Michigan	Salina Group F1	86ND101-ND1		Extraction-IC	1970	350	1560	730	6530		31.3		5.5	63.3	7.1		29.6
	Michigan	Salina Group F1	86ND101-ND2		Extraction-IC	1480	410	1840	930	7770		31.5		−4.5	61.8	6.9		31.3
	Michigan	Salina Group F1	86ND101-ND3		Extraction-IC	1050	370	2050	950	7550		46.2		−1.7	64.4	5.8		29.8
	Michigan	Salina Group F1	86ND101-ND4		Extraction-IC	1390	370	1960	920	7170		45.0		4.8	63.9	6.0		30.0
	Michigan	Salina Group F1	86ND101-ND5		Extraction-IC	750	460	2340	1100	7200		43.9		11.6	63.8	6.3		30.0
sw	Michigan	Salina Group F1	86ND101-ND6		Extraction-IC	1320	490	1470	1410	7840		48.7		−3.5	47.0	7.8		45.1
	Michigan	Salina Group F1	86ND103-ND7	ch	Extraction-IC	960	490	1750	1310	7500		53.3		0.9	53.0	7.4		39.6
sw?	Michigan	Salina Group F1	86ND103-ND8	ch	Extraction-IC	880	490	1990	1020	7690		40.4		−4.0	61.1	7.5		31.3
sw?	Michigan	Salina Group F1	86ND103-ND9	ch	Extraction-IC	950	500	2070	1040	7460		44.2		2.8	61.6	7.4		31.0
	Michigan	Salina Group F1	86ND103-ND10	ch	Extraction-IC	1000	540	2220	1050	8060		51.9		0.2	62.7	7.6		29.7
sw?	Michigan	Salina Group F1	86ND103-ND11	ch	Extraction-IC	860	510	2220	1040	7700		43.6		2.4	63.2	7.3		29.6
sw?	Michigan	Salina Group F1	86ND103-ND12	ch	Extraction-IC	1040	540	2220	970	8000		41.8		−0.5	64.2	7.8		28.0
	Michigan	Salina Group F1	86ND104-ND13	ch	Extraction-IC	1000	460	2130	1110	7200		46.5		9.8	61.4	6.6		32.0
sw?	Michigan	Salina Group F1	86ND104-ND14	ch	Extraction-IC	960	480	2030	920	7000		40.2		4.7	63.6	7.5		28.8
	Michigan	Salina Group F1	86ND104-ND18	ch	Extraction-IC	850	460	1630	1910	9580		41.3		−13.2	43.2	6.1		50.7
sw*	Michigan	Salina Group F1	86ND105-ND15		Extraction-IC	1830	460	1280	740	6210		35.0		1.9	56.9	10.2		32.9
sw*	Michigan	Salina Group F1	86ND105-ND16		Extraction-IC	1650	420	1520	830	6220		31.3		8.5	59.4	8.2		32.4
sw?	Michigan	Salina Group F1	86ND105-ND17		Extraction-IC	1780	410	1590	890	7380		34.9		−3.2	59.2	7.6		33.1
					Lower Silurian: Carribuddy Formation, Australia (this study)													
	Australia	Carribuddy	Car12-3-3-1		Extraction-IC	167	280	4750	1060	11600		80.6		3.9	79.8	2.4		17.8
	Australia	Carribuddy	Car12-2-3-1		Extraction-IC	107	44.6	3250	3310	13600		108		−2.4	49.4	0.3		50.3
	Australia	Carribuddy	Car12-3-2-1		Extraction-IC	130	77	2990	2990	11200		80.2		8.3	49.7	0.6		49.7
	Australia	Carribuddy	Car12-3-2-2		Extraction-IC	177	175	2780	2620	10500		76.7		6.0	50.7	1.6		47.7
	Australia	Carribuddy	Car12-2-2-1		Extraction-IC	107	77.6	2940	2880	10600		85.5		10.9	50.2	0.7		49.2
	Australia	Carribuddy	Car12-3-2-3		Extraction-IC	261	357	2500	2480	10200		71.3	5	3.6	48.5	3.5		48.1
	Australia	Carribuddy	Car12-4-4-1		Extraction-IC	222	239	2750	2530	10600		74.9	4	3.9	50.9	2.2		46.9
					Early Cambrian: E Siberian Platform (this study)													
	Siberia		Sib1-2	ch	Extraction-IC	438	435	3070	1250	9330		55.4	26	1.9	67.7	4.8		27.5
	Siberia		Sib1-3	ch	Extraction-IC	474	437	2920	1170	8840		41.7	25	2.8	67.8	5.1		27.2
	Siberia		Sib1-4	ch	Extraction-IC	257	293	2390	2520	10000		67.8	29	3.6	47.3	2.9		49.8
	Siberia		Sib1-5	ch	Extraction-IC	1910	279	1320	950	6680		29.2	14	0.7	54.8	5.8		39.4
	Siberia		Sib2-1	ch	Extraction-IC	446	591	3150	1180	9610		63.8	16	0.9	68.1	6.4		25.5

(Continued)

Appendix. (Continued)

	Stratigraphy/basin	Sample	Inclusion type	Method	Na	K	Mg	Ca	Cl	SO_4	Br	Li	CB	Mg	2K	SO_4	Ca
					(mmol/kg H_2O)								(%)	Jänecke unit (%)			
				Early Cambrian: E Siberian Platform (this study)													
	Siberia	Sib2-2	ch	Extraction-IC	470	639	3080	1020	9070		46.2	12	2.6	69.7	7.2		23.1
	Siberia	Sib2-3	ch	Extraction-IC	457	619	3180	1100	9430		61.3	12	2.2	69.3	6.7		24.0
	Siberia	Sib2-4	ch	Extraction-IC	437	570	3100	1100	9300		69.8	13	1.1	69.1	6.4		24.5
	Siberia	Sib2-5	ch	Extraction-IC	604	707	2870	930	8770		82.3	13	1.6	69.1	8.5		22.4
	Siberia	Sib2-6	ch	Extraction-IC	443	565	3040	1300	9330		61.1	16	3.8	65.8	6.1		28.1
	Siberia	Sib4-1	ch	Extraction-IC	361	475	2860	1510	9100		48.8	16	5.1	62.1	5.2		32.8
	Siberia	Sib4-2	ch	Extraction-IC	389	542	2740	1570	9050		41.6	14	5.4	59.8	5.9		34.3
	Siberia	Sib4-3	ch	Extraction-IC	387	595	2460	1830	9410		42.7	15	1.6	53.6	6.5		39.9
	Siberia	Sib4-4	ch	Extraction-IC	406	527	2790	1540	9380		30.1	16	2.2	60.7	5.7		33.5
	Siberia	Sib4-5	ch	Extraction-IC	410	608	2520	1930	10400		54.4	15	−4.7	53.0	6.4		40.6
	Siberia	Sib5-1		Extraction-IC	398	349	2720	1690	9790		61.4	27	−2.3	59.3	3.8		36.9
	Siberia	Sib5-2		Extraction-IC	401	355	2870	1670	9870		30.7	22	−0.3	60.8	3.8		35.4
	Siberia	Sib5-3		Extraction-IC	336	318	2880	1650	9850		75.0	28	−1.4	61.4	3.4		35.2
				Late Neoproterozoic: Ara Formation, Oman (this study)													
	Oman	7-1	ch	Extraction-IC	493	589	4420		8530	410	69.3	9	5.9	86.3	5.7	8.0	
	Oman	7-2	ch	Extraction-IC	500	570	4530		8950	436	79.8	10	3.1	86.3	5.4	8.3	
sw?*	Oman	7-3	ch	Extraction-IC	405	421	4700		7795	761	58.2	14		82.9	3.7	13.4	
sw?*	Oman	7-4	ch	Extraction-IC	486	565	4340		8590	407	55.9	14	3.4	86.3	5.6	8.1	
	Oman	7-5	ch	Extraction-IC	499	587	4610		8890	456	69.9	11	5.0	86.0	5.5	8.5	
	Oman	7-7	ch	Extraction-IC	476	555	4490		8980	465	68.0	11	1.0	85.8	5.3	8.9	
	Oman	7-8	ch	Extraction-IC	430	532	4380		8510	382	65.2	11	4.7	87.1	5.3	7.6	
	Oman	7-9	ch	Extraction-IC	491	619	4320		8640	443	66.1	11	2.3	85.2	6.1	8.7	
	Oman	7-10	ch	Extraction-IC	477	581	4270		8500	360	72.6	14	4.0	86.8	5.9	7.3	
	Oman	7-11	ch	Extraction-IC	483	553	4410		8120	394	64.1	14	10.1	86.8	5.4	7.8	

[a] sw, seawater evaporated before potash facies on the basis of saturation index calculations with Harvie et al. (1984) model and screening criteria of Zimmermann (2001); *inclusions used to reconstruct the composition of seawater (Tables 1 and 2, Figs. 5–10); ch, inclusions within or adjacent to chevron halite; CB, charge balance = $[100 \times (\Sigma_{cations} - \Sigma_{anions})/0.5 \times (\Sigma_{cations} + \Sigma_{anions})]$.